LEVEL II

12

ADA078435

OCEAN CITY RESEARCH CORP.
TENNESSEE AVE. & BEACH THOROFARE
OCEAN CITY, NEW JERSEY 08226

CORROSION OF ALUMINUM ALLOYS IN HIGH VELOCITY SEAWATER

BY

G. A. GEHRING, JR.

FINAL REPORT

PREPARED FOR

DEPARTMENT OF THE NAVY
OFFICE OF NAVAL RESEARCH
METALLURGY PROGRAM - CODE 471

NOVEMBER, 1979

Unclassified

SECURITY CLASSIFICATION OF THIS PAGE (When Data Entered)

REPORT DOCUMENTATION PAGE		READ INSTRUCTIONS BEFORE COMPLETING FORM
1. REPORT NUMBER	2. GOVT ACCESSION NO.	3. RECIPIENT'S CATALOG NUMBER
4. TITLE (and Subtitle) (6) CORROSION OF ALUMINUM ALLOYS IN HIGH VELOCITY SEAWATER, (14)		5. TYPE OF REPORT & PERIOD COVERED: Final, 7/78 to 7/79
		6. PERFORMING ORG. REPORT NUMBER: OCR-ONR-3
7. AUTHOR(s) (10) G. A. Gehring, Jr.		8. CONTRACT OR GRANT NUMBER(s) (15): N00014-78-C-0720
9. PERFORMING ORGANIZATION NAME AND ADDRESS: OCEAN CITY RESEARCH CORP. TENNESSEE AVE. & BEACH THOROFARE OCEAN CITY, N.J. 08226		10. PROGRAM ELEMENT, PROJECT, TASK AREA & WORK UNIT NUMBERS
11. CONTROLLING OFFICE NAME AND ADDRESS: OFFICE OF NAVAL RESEARCH METALLURGY PROGRAM OFFICE, CODE 471 ARLINGTON, VIRGINIA 22217 (11)		12. REPORT DATE: Nov[redacted]79
		[redacted] NUMBER OF PAGES
14. MONITORING AGENCY NAME & ADDRESS (if different from Controlling Office)		15. SECURITY CLASS. (of this report): Unclassified
		15a. DECLASSIFICATION/DOWNGRADING SCHEDULE

16. DISTRIBUTION STATEMENT (of this Report)

Approved for public release; distribution unlimited. Reproduction in whole or in part is permitted for any purpose of the United States Government.

17. DISTRIBUTION STATEMENT (of the abstract entered in Block 20, if different from Report)

(9) Final rept. Jul 78-Jul 79,

18. SUPPLEMENTARY NOTES

(12) 46

19. KEY WORDS (Continue on reverse side if necessary and identify by block number)

Corrosion, High Velocity, Seawater, Aluminum

20. ABSTRACT (Continue on reverse side if necessary and identify by block number)

A study was undertaken to examine the corrosion behavior of selected aluminum alloys in high velocity seawater. The work is pertinent to the development of high speed ships by the U.S. Navy. The selected aluminum alloys included 1100-H14 and 5456-H117. Plate specimens of each alloy were exposed in a flow channel at test velocities ranging from 3 to 30 m/s. The affect of cathodic polarization on the

DD FORM 1 JAN 73 1473 EDITION OF 1 NOV 65 IS OBSOLETE S/N 0102-LF-014-6601

Unclassified 409 286

SECURITY CLASSIFICATION OF THIS PAGE (When Data Entered)

20.

velocity-related corrosion behavior of the 5456 alloy was also investigated. The flow channel uses natural seawater and is capable of achieving any velocity between 0 and 30 m/s under turbulent, high Reynolds Number ($Re > 10^6$) flow conditions.

Under the flow conditions established in the study, the results show that: (1) both the rate and mode of corrosion are velocity-dependent for aluminum alloys (2) velocity-related shifts in corrosion potential can occur (3) polarization resistance measurements are inadequate for predicting corrosion rates of aluminum alloys in high velocity flow (4) cathodic protection cannot retard velocity-induced corrosion of aluminum alloys (5) cathodic polarization will tend to accelerate corrosion of aluminum alloys at all velocities tested (6) at higher velocities, the predominant reduction reaction associated with the corrosion of aluminum alloys is $H_2O + 1e \rightarrow OH^- + 1/2\ H_2$.

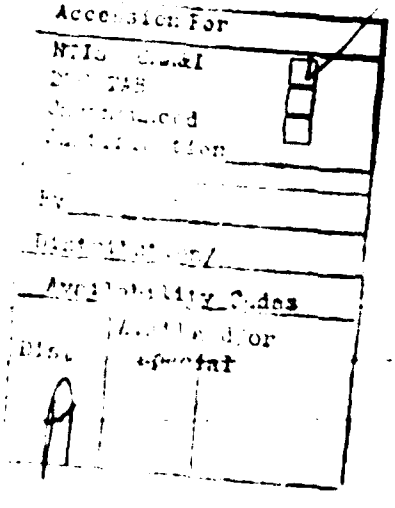

CORROSION OF ALUMINUM ALLOYS IN HIGH VELOCITY SEAWATER

BY

G. A. GEHRING, JR.

FINAL REPORT

PREPARED FOR

DEPARTMENT OF THE NAVY
OFFICE OF NAVAL RESEARCH
METALLURGY PROGRAM - CODE 471

NOVEMBER, 1979

ABSTRACT

A study was undertaken to examine the corrosion behavior of selected aluminum alloys in high velocity seawater. The work is pertinent to the development of high speed ships by the U.S. Navy. The selected aluminum alloys included 1100-H14 and 5456-H117. Plate specimens of each alloy were exposed in a flow channel at test velocities ranging from 3 to 30 m/s. The affect of cathodic polarization on the velocity-related corrosion behavior of the 5456 alloy was also investigated. The flow channel uses natural seawater and is capable of achieving any velocity between 0 and 30 m/s under turbulent, high Reynolds Number ($Re > 10^6$) flow conditions.

Under the flow conditions established in the study, the results show that: (1) both the rate and mode of corrosion are velocity-dependent for aluminum alloys (2) velocity-related shifts in corrosion potential can occur (3) polarization resistance measurements are inadequate for predicting corrosion rates of aluminum alloys in high velocity flow (4) cathodic protection cannot retard velocity-induced corrosion of aluminum alloys (5) cathodic polarization will tend to accelerate corrosion of aluminum alloys at all velocities tested (6) at higher velocities, the predominant reduction reaction associated with the corrosion of aluminum alloys is $H_2O + 1e \rightarrow OH^- + 1/2\ H_2$.

INTRODUCTION

A study was undertaken to examine the corrosion behavior of selected aluminum alloys in high velocity seawater. The work is pertinent to the development of high speed ships by the U.S. Navy. It is anticipated that these ships (e.g. Surface Effect Ships) might approach operating speeds of ≈ 50 m/s (≈100 knots)

EXPERIMENTAL APPROACH

The study was accomplished using a flow channel available at the Ocean City Research Corporation laboratory. The flow channel is designed to permit velocity testing under conditions that are reasonably representative of conditions that would exist over a major portion of a high speed ship hull (parallel, turbulent, high Reynolds Number flow). The flow channel accommodates comparatively larger test panels, thus tending to minimize edge and/or boundary effects. Test panels were prepared from certified aluminum alloy plate of 5456-H117 and 1100-H14. Table I presents the typical composition of the 5456 alloy. The 1100 alloy is commercially pure (99.0+0/0 Al).

Flow Channel Description

Figure 1 shows the OCRC flow channel. The width of the channel cross-section varies along the length to permit testing at 6 different flow velocities simultaneously (maximum velocity 18 m/s). A separate, constant-width section permits testing at higher velocities (maximum velocity ≈ 30 m/s). Figure 2 presents a simplified schematic of the channel. For the present study, the nominal test velocities were 30, 18, 15, 12, 9, 6 and 3 m/s, respectively.

Figure 3 shows the method by which test panels were mounted in the low velocity section (3 m/s thru 18 m/s) of the channel. Each velocity subsection accommodated 5 test panels (17.5 cm x 25.5 x cm ≈ 1.3 cm thick). The test panels were spaced 5 cm apart using acrylic spacers to maintain a continuous center wall in each section. The interface between spacer and panel was matched as precisely as possible to avoid edge effects. Electrical leads were attached to some test panels to permit electrochemical potential and polarization measurements.

The high velocity test section was fabricated from 1-inch thick acrylic plastic with a flow channel cross section of 2.5 cm x 20.3 cm. The test section was 122 cm long. The test section accommodated eight 15.2 cm x 25.4 cm x 1 cm thick panels, four per each wall of the channel. Figure 4 shows the general arrangement on each wall of the channel. The test panels were flush-mounted and carefully shimmed to minimize edge mismatch and eliminate cavitation. The panels were held in place by studs tapped into the back of the panel. These served the additional purpose of allowing electrical connections to be made for electrochemical measurements.

Natural seawater is circulated through the channel by a double-suction centrifugal pump powered by a 100 H.P. motor. The flow rate can exceed 300 l/s and is measured using a factory-calibrated 316 SS orifice plate/differential pressure gauge set-up. The rate of seawater make-up into the channel is adjusted to control seawater temperature within ± 2.5°C while being maintained sufficiently high to avoid stagnation or concentration effects. For the present study, the make-up rate varied between 2 and 5 l/s.

The channel was designed to provide high Reynolds Number flow at each test velocity ($Re \approx 10^6$). This was done in order to better simulate flow conditions that might be encountered during high speed ship operation.

Test Conditions

Data was obtained over four separate test runs in the flow channel. Table II summarizes the conditions for each test run. Data acquisition throughout the test runs included electrochemical potential and polarization measurements, weight loss measurements and pit depth measurements. In addition, the exposed panels were examined in detail using both an optical and a Scanning Electron Microscope. Electrochemical data were obtained utilizing techniques which are adequately described in the literature. Weight loss data were obtained using an analytical balance accurate to ± 0.5 gm. Data was obtained daily on seawater samples from the channel, including temperature, salinity, dissolved oxygen concentration, pH and turbidity.

Measurements of Limiting Oxygen Diffusion Current Vs Velocity

A platinum electrode was also exposed in each velocity subsection in order to determine limiting oxygen diffusion currents as a function of velocity. Figure 5 depicts the method used to prepare and mount the platinum electrodes. 500 mm. long x 3 mm. wide x .127 mm. thick strips of platinum foil were cigarette-rolled and then cast in acrylic resin so as to expose only the edge. The acrylic-cast platinum was then polished on the exposed edge side and solvent-cemented flush in the side wall of the channel. The mounted specimen was re-polished so as to provide a smooth surface with minimal mismatch between the platinum and the acrylic.

RESULTS AND DISCUSSION

Corrosion Rate Versus Velocity

Figure 6 presents a semi-log plot of corrosion rate versus velocity for the 5456 and 1100 alloys. At the lower test velocities, the 1100 alloy corroded at a higher rate than the 5456 alloy. Corrosion rates could not be determined for the 5456 alloy at the two lowest test velocities (3 m/s, 6 m/s) because

the weight loss for the test panels at these velocities was below the sensitivity of the balance used to weigh the panels. The use of large, relatively heavy panels (≈2000 gm) necessitated the use of a relatively insensitive balance (sensitivity = ±.5 gms). At the highest velocity (30 m/s), the 5456 alloy exhibited a higher corrosion rate.

Previous work[1] involving just the 5456 alloy indicated that there might be a characteristic "breakaway" velocity associated wth the 5456 alloy. The so-called "breakaway" velocity as defined by Efird[2] for copper-nickel alloys is the velocity where corrosion increases sharply due to velocity-associated breakdown or rupture of the protective film on the surface of the metal. In earlier work, the 5456 alloy showed a sharp transition in the corrosion rate versus velocity plot at 9 m/s. However, the results of the more recent study were inconclusive relative to this hypothesized breakaway velocity because of the inability to determine corrosion rates at the lower velocities. The corrosion rate-velocity plot for the 1100 alloy did not evidence a characteristic breakaway velocity.

A log-log plot (Figure 7) of the same data plotted in Figure 6 suggests that at the higher velocities, corrosion rate-velocity dependence is best approximated as follows:

$$\text{corrosion rate} = k\, V^{3.6}$$

Many investigators have suggested that the velocity-related increase in corrosion rate of most common alloys in neutral salt solutions should correspond to the increase in limiting oxygen diffusion current with velocity. From purely theoretical considerations, the consensus of opinion in the literature is that the limiting oxygen diffusion current should be proportional to $V^{.6}$ to $.9$ under conditions of turburlent flow. The data obtained as part of this study strongly suggest that at higher velocities in turburlent, high Reynolds Number flow, there are other factors (than just the diffusion rate of dissolved oxygen) that will exert a primary influence on the corrosion rate of aluminum alloys.

Morphological Aspects

In an earlier paper[1], this author documented changes in surface morphology for the 5456 alloy as a function of velocity. At lower velocities, the hydrated oxide layer(s) which typically formed in seawater were observed to be stable. Corrosion occurred primarily in the form of localized macropitting as has been observed by many other investigators. However, at higher velocities (≈ 9 m/s), the 5456 alloy corroded in a fashion considered to be unusual for aluminum alloys. On a macroscopic scale, corrosion appeared to occur uniformly, resulting in a smooth, shiny surface even though the rate was very high. On a microscopic scale, localized pitting was observed about intermetallic particles in the 5456 alloy matrix. The pits were elongated in

the direction of flow downstream of the intermetallic particles. Figure 8 shows the macroappearance of the test panel while Figure 9 is an SEM micrograph showing typical pitting about the intermetallic particles.

Based on these observations, a high velocity mode of corrosion was hypothesized for the 5456 alloy. Pit initiation occurs at intermetallic particles, probably because the film is less protective at these points and because of the galvanic action between the aluminum matrix and more noble intermetallic particles. At the same time, general metal loss on the surface causes the intermetallic particles to protrude into the flow stream. Up until this point, pitting occurs uniformly about the intermetallic particle. However, with the intermetallic particles protruding increasingly into the flow stream, pitting begins to breakout and occur much more rapidly downstream of the particles. This occurs because of the localized increase in turbulence immediately downstream of the particles and possibly, due to a localized pH effect. The pH effect could occur as the result of the hydrolysis of metastable $AlCl_4$ hypothysized by Becerra and Darby as follows:

$$2\ AlCl_4^- + 6\ H_2O \rightarrow Al_2O_3.3H_2O + 6H^+ + 8\ Cl_4^-$$

The H^+ ions can then be swept downstream causing a localized drop in pH and subsequent dissolution of the oxide film. Eventually, the intermetallic particle is undermined and removed by hydrodynamic shear stresses. Once the intermetallic particle is gone, the galvanic cell no longer exists and the rate of pitting corrosion increases. Flow stagnation in the remaining depression results in a corrosion rate lower than the rest of the surface. This process, repeated over and over, results in relatively uniform metal loss which, macroscopically, gives a very smooth surface appearance. Figure 10 illustrates the hypothesized behavior in step-wise fashion.

Test panels of the 5456 alloy, exposed again as part of the subject study, also evidenced this morphological behavior. Examination of the 1100 alloy panels, however, revealed different morphological characteristics. At 30 m/s, the macroscopic appearance of the 1100 alloy test panels was smooth and shiny, similar to the 5456 alloy. However, microscopically, the alloy exhibited crystallographic, etch-like pits instead of preferential pitting around intermetallic particles. Figures 11 and 12 show the macroscopic and microscopic appearance of the 1100 alloy panel after exposure at high velocity.

At 18 m/s, the 1100 alloy exhibited a much rougher surface than the 5456 alloy. The rougher surface was the result of small blister-like protuberances which were distributed uniformly over the surface. These blisters were clearly visible to the naked eye and appeared to consist of blistered metal as well as mounds of corrosion product. Figure 13 shows an 1100 alloy panel as well as a 5456 alloy panel for comparison.

Examination of the test panels exposed at lower velocities (15 m/s through 3 m/s) showed that with decreasing velocity the blister-like protuberances increased in size (from ≈ 1.5 mm in diameter @ 18 m/s to ≈ 3 mm in diameter @ 3 m/s) but decreased in the number per unit surface area. Also, with decreasing velocity, the protuberances began to appear less like blistered metal and more like mounds of corrosion product, similar to what is observed on panels exposed in quiescent seawater.

The susceptibility of the 1100 alloy to blistering as part of the corrosion process was reported by Draley and Ruther[10]. Draley and Ruther exposed 1100 alloy specimens in distilled water at various elevated temperatures and observed an increasing tendency for blistering with an increase in temperature. These authors hypothesized that the blisters occurred as a result of hydrogen reduction during the corrosion reaction. They proposed that hydrogen ions were reduced to atomic hydrogen at the metal-oxide interface, diffused into the metal, then recombined to form hydrogen molecules causing a localized build-up of pressure at voids in the lattice. Subsequently, blistering occurred.

Draley and Ruther also showed that alloying aluminum with metals having a low hydrogen overvoltage diminished the tendency for blistering. The alloying metals form compounds which are more noble than the aluminum matrix and are preferred sites for the hydrogen reduction reaction. Hydrogen produced at these sites presumably diffuses or bubbles into solution. However, it is doubtful whether the lower hydrogen overpotential of alloying elements is responsible for the lack of blistering on the 5456 alloy. Potential and polarization data, presented later in this paper, suggest that the 5456 alloy has a greater hydrogen overpotential than the 1100 alloy. It is not clear why the 1100 alloy blistered at 18 m/s and the 5456 alloy did not. Both alloys had close to the same corrosion rate. The difference in degree of observed blistering may be associated with the difference in strength of the two alloys. The 100 alloy has a lower yield strength (117. x 10^3 kps vs. 165. x 10^3 kpa) and it seems reasonable, therefore, that blistering might occur at lower local hydrogen pressures.

Microscopic inspection of the 1100 alloy panels exposed at 18 m/s revealed hemispherical non-crystallographic micropitting (Figure 14) as opposed to the distinct crystallographic pitting observed at 30 m/s. The change in pit morphology in going from 18 to 30 m/s is thought to occur as a result of the greater breakdown of the oxide film with increasing velocity and corresponding increase in corrosion rate. Typically, pure metals exhibit crystallographic etch pits in highly reactive etching solutions where the rate of metal dissolution is high. Seawater moving at high velocity (≈ 30 m/s) also causes a high rate of metal dissolution and the resulting surface morphology is similar to what might occur in a highly reactive reagent. The absence of hydrogen caused blisters at 30 m/s also probably relates to the

breakdown or thinning of the oxide film as velocity increases. In discussing the possible mechanism for hydrogen blistering, Draley and Ruther suggested that diffusion of hydrogen molecules back into solution would be hindered by the oxide film at the metal oxide interface, thus prompting hydrogen diffusion into the metal matrix. The lack of blistering at 30 m/s suggests that the back-diffusion barrier (oxide film) has been eliminated or greatly reduced.

Electrochemical Behavior Versus Velocity

Figure 15 shows the corrosion potential for both alloys plotted against velocity. These data represent the mean corrosion potentials obtained from Test Run #3. Data from the separate 30 m/s test is not included because this test was conducted at a warmer water temperature. As observed in earlier work, the 5456 alloy again exhibited an active shift in potential with increasing velocity. It was postulated previously that the active shift in potential was caused by increases in the anodic diffusion-limited current density. The increase in anodic diffusion-limited current density occurs as the result of oxide breakdown with increasing velocity. Figure 16 is a polarization diagram demonstrating how the active shift could occur in such a fashion.

While the 5456 alloy exhibited a marked potential shift with velocity, there appeared to be only a slight shift, if at all, for the 1100 alloy. At the lowest velocity (3 m/s), the 1100 alloy was approximately 40 millivolts more noble than the 5456 alloy which agrees with published data[11] on these alloys obtained under quiescent conditions. The corrosion potential exhibited by the 1100 alloy is in the range of the critical pitting potential generally associated with this alloy. This seems reasonable considering the magnitude of measured corrosion rates and pitting that was observed. A lower hydrogen overpotential on the 1100 alloy would explain the absence of a significant shift in potential compared to the 5456 alloy.

Polarization data was obtained throughout the velocity test, including full anodic and cathodic polarization scans as well as polarization resistance measurements or so-called "linear" polarization measurements. At the high velocities, corrosion rates calculated from the polarization resistance measurements were considerably less than corrosion rates determined by weight loss. Table III summarizes some of this data.

Corrosion rates were calculated from the polarization resistance measurements using the Stern-Geary technique as later modified by Mansfeld[13]. Tafel constants (βa & βc) were estimated according to the curve fitting method suggested by Mansfeld because full anodic and cathodic polarization curves did not yield unambiguous Tafel slopes. The Tafel constants estimated from the polarization resistance curves suggested βa & βa = .120 represented a reasonable approximation for all velocities.

The shape of the polarization resistance curves did not change significantly as a function of velocity.

At the higher velocities, Table III shows that corrosion rates determined by polarization resistance are close to an order of magnitude lower than the weight loss rates. At lower velocities, there appears to be reasonable agreement.

Consideration of the criteria necessary for valid application of the polarization resistance technique does not provide a clear-cut answer why such a large difference should exist. The polarization response to a current step observed on an oscilloscope indicated that ohmic voltage drops were not present and thus could not account for the error. It is possible that concentration polarization is present, however, the possible degree of error associated with concentration polarization effects ($\beta a = \infty$ or $\beta c = \infty$) doesn't appear sufficient to account for the observed difference. It is also possible that the equilibrium potential for the reduction reaction is too close to the corrosion potential. However, the error arising from the close proximity of the half-cell redox potential to the corrosion potential results in predicted corrosion rates that are higher than those determined by weight loss as shown by Mansfeld and Oldham[14]. This is opposite to what was obtained. In the same respect, the difference doesn't appear attributable to a secondary reaction effect.

The possiblity was also considered that the difference reflects weight loss associated with purely hydromechanical wear not detectable by the polarization resistance technique. While there was certainly evidence of intermetallic particle removal by purely hydromechanical forces, there was no evidence of selective grain boundary attack which would result in whole grain dropping. The hydromechanical removal of intermetallic particles can't account for the difference. Furthermore, the possibility of removing base metal by hydromechanical wear is discounted because of other work[15] conducted by this author where solvent-type coating materials exhibited negligible weight loss under identical exposure conditions. The cohesive strength of the coating materials is certainly less than the cohesive strength of the 5456 alloy. Thus, the reason for the observed difference, remains uncertain.

One possible explanation for the discrepancy with respect to polarization-determined corrosion rates might be that at high velocities the disruption of the aluminum oxide film occurs to such an extent that the highly reactive aluminum base metal is exposed permitting spontaneous interaction with the environment without transport of charge. However, further investigation is required to determine the exact cause for the discrepancy in the polarization-determined corrosion rates.

Figures 17 and 18 show representative cathodic polarization curves for the 5456 and 1100 alloys obtained at different

velocities. The curves do not show unambiguous Tafel slopes, making the determination of corrosion rates by Tafel slope back-extrapolation impossible. The polarization scans also failed to show meaningful differences as a function of velocity. For example, the scans on the 1100 alloy were almost indistinguishable as a function of velocity and, in fact, there was a slight tendency for cathodic polarization to occur more readily as velocity increased.

Effect of Cathodic Protection

The possibility of retarding velocity-induced corrosion by cathodic protection was investigated. Test panels of the 5456 alloy galvanically coupled to zinc anodes (anode-to-cathode area ratio = 1:2) were exposed at each test velocity. Also, additional test panels of the 5456 alloy were cathodically polarized at substantially higher cathodic current densities than obtainable with zinc anodes by using an impressed current system. Currents to each test panel were monitored in all cases. Potentials of all zinc-coupled panels were also monitored throughout the tests. Potential measurements on panels cathodically polarized with the impressed current system were not possible because the reference electrode could not be located in close proximity to the test panels. Potential measurements with a remote electrode picked up significant "IR" drop.

Figure 19 shows the effect of coupling zinc anodes to the 5456 test panels. At every velocity, the corrosion rate increased. *Thus, cathodic protection with zinc anodes has no* beneficial effect and appears to cause a slight increase in corrosion rate.

Figures 20 and 21 show the variation in potential and current of each zinc-coupled 5456 panel over the course of the test. Initially, zinc-coupled aluminum panels polarized close to the open circuit potential generally associated with zinc in seawater (-1.05 volts vs. SCE). The current density averaged over the 6 test velocities was approximately .06 ma/cm , which is a much lower current density than zinc anodes normally are designed to operate. Initially, there was no significant difference in either potential or current attributable to velocity. This tends to corroborate the results of the electrochemical polarization measurements which suggested the polarization behavior of the 5456 alloy was insensitive over this velocity range.

Over the course of the test, the potential of the zinc-coupled panels tended to shift to more electropositive values. Generally, the shift was between 15 and 150 millivolts with the largest shifts occurring at the higher velocities. However, for the most part, there was not a significant increase in current corresponding to the observed potential shift. The lack of significant current increase as the zinc/aluminum couples shifted toward more noble potential values suggests possible

passive film formation on the zinc anodes. This would be contrary to the results of work by Perkins et al[16] conducted at higher anodic current densities but lower velocities.

The test panels exposed at the lower velocity exhibited a thin copper-like film (Figure 22) in marked contrast to the oxide film formed under freely corroding conditions. Qualitative analytical chemical tests confirmed the presence of iron and copper on the surface at the lower velocities. Copper and iron are present in seawater, generally at concentrations below .01 ppm. The qualitative chemical tests failed to detect the presence of copper or iron on the surface of test panels exposed at the higher velocities. The test panels at higher velocities exhibited the same bright, shiny appearance as observed on the freely corroding panels. SEM examination also showed a similar surface morphology as reported for the freely corroding panels. The absence of copper or iron at detectable levels at the higher velocities suggests that corrosion of the aluminum substrate is proceeding at a much faster rate than the rate at which iron or copper tend to electrodeposit because of the galvanic coupling with zinc.

At the higher impressed current densities, an experimental problem was encountered in that zinc from the dissolving anodes plated out on downstream test panels. This was especially noticeable at lower velocities. In general, where zinc plating was not detectable, higher impressed current densities caused higher corrosion rates, without a noticeable change in the observed morphology of corroding surface previously reported. Where zinc plating occurred, corrosion rates tended to be lower. Table IV summarizes data obtained at 3 m/s through 18 m/s.

At 30 m/s, two test panels were exposed under constant potential conditions (-1.40 and -1.80 volts versus SCE). The corresponding average current densities over the course of the tests were 3,360 and 4,370 $\mu amps/cm^2$, respectively. At the highest potential, the test panel was severely corroded, averaging a rate of 382 mdd over the test period. The test panel held at a potential of -1.40 volts corroded at less than 1.5 mdd over the test. Upon removal from the test, the panel exhibited a dense black film approximately 4 mils in thickness. Energy Dispersive X-ray analysis showed that the film consisted primarily of zinc with some copper. As reported above, the source of the electrodeposited zinc was the zinc anodes dissolving upstream. Considering the results at lower velocities, it is assumed that polarization of the 5456 alloy to a potential of -1.40 volts in the absence of zinc-contaminated seawater would result in a higher corrosion rate than normally occurs under freely corroding conditions.

Cathodic polarization of the 5456 alloy caused higher corrosion rates than under freely corroding conditions in all cases except the one noted above. This demonstrates clearly that even at high seawater velocities, cathodic polarization can

create the alkaline conditions that will accelerate corrosion of aluminum alloys. There had been some conjecture as to whether a localized increase in alkalinity could occur at the metal/liquid interface under conditions of high velocity, turbulent flow. Also, the results show the ineffectiveness of using cathodic protection to retard velocity-induced corrosion of aluminum alloys. In quiescent waters, cathodic protection can successfully be used to prevent pitting of aluminum by polarizing the alloy to a more active value than its pitting potential. However, in high velocity, turbulent flow, cathodic protection is ineffective. The results also provide additional evidence that corrosion of aluminum in high velocity seawater proceeds in a different fashion than the classical behavior associated with a quiescent situation.

Limiting Oxygen Diffusion Current Versus Velocity

As previously referenced, many investigators have suggested that corrosion in high velocity seawater flow is controlled by mass transfer in the seawater, specifically the migration of dissolved oxygen to the metal surface where it undergoes cathodic reduction. There have been several analytical treatments where expressions relating mass transfer limited diffusion current, I_ℓ, to velocity have been developed. The most widely referenced work is that of Levich [16]. Levich treated both laminar and turbulent flow and showed from theoretical considerations that:

$$I_\ell = k\ V^{.5} \text{ for laminar flow}$$

and,

$$I_\ell = k\ V^{.8 \text{ to } .9} \text{ for turbulent flow}$$

Experimental verification of the laminar flow relationship is good, however verification of the relationship for turbulent flow has not been documented for high velocity (10-30 m/s), high Reynolds Number ($\simeq 10^6$) flow.

In previous work, Davis and Gehring[17] derived an equation showing I_ℓ to be proportional to $V^{.2}$ in high velocity turbulent flow. Davis and Gehring used the equation $Sc^{1/3} = d_h/d_d$ which defines the relationship between the mass transfer boundary layer, d_d, and the hydrodynamic boundary layer, d_h, in terms of the Schmidt number, Sc, a dimensionless parameter. The Schmidt number represents the ratio of the kinematic viscosity, , to the diffusion coefficient, D. This relationship allowed I_ℓ to be related to flow velocity using Reynold's analogy. Leumer et al[18] have since suggested that the relationship derived by Davis and Gehring is invalid because $Sc^{1/3} = d_h/d_d$ is not valid in turbulent flow. Leumer further suggests that a more appropriate relationship would be one derived by Wranglen[19]:

$$I = .143\ ZFDc_b Re_x^{.6} : [(1-n)x]Sc^{.33}$$

Where,

Z = Valence
F = Faraday's constant
D = Diffusion coefficient
c_b = Concentration of diffusing species
R_{e_x} = Reynolds number for characteristic length x
x = characteristic length
n = Number of electrons transferred
Sc = Schmidt number

From Wranglen's equation, I_ℓ is proportional to $V^{.6}$.

Cathodic polarization measurements were made on platinum electrodes in quiescent seawater and over a range of seawater velocities. The results of these measurements are shown in Figure 23. The limiting diffusion density in quiescent seawater was about 100 amps/cm , in reasonable agreement with the literature for the following reaction:

$$1/2\ O_2 + H_2O + 2e \rightarrow 2(OH)^-$$

Under turbulent flow, a limiting diffusion current was only observed at the two lowest test velocities i.e. 3 m/s and 6 m/s, respectively. At 3 m/s, the limiting diffusion current was approximately 75 $\mu amps/cm^2$, which is slightly lower than the diffusion current measured under quiescent conditions. As a first impression this would seem to be highly improbable and cast some doubt on the validity of the experimental methods. However, inspection of the platinum surface at 3 m/s (as well as the remainder of the exposed surfaces in this section of the channel) showed that a slime/silt film had formed during the 779-hour seawater exposure. The polarization measurements were made after approximately 750 hours in test. Thus, at 3 m/s, the presence of the slime film undoubtedly influenced the measured diffusion current. A slime film was not detected at higher velocities. In quiescent seawater, the measurements were made immediately after exposure on a slime-free surface.

The limiting oxygen diffusion current measured at 6 m/s agrees reasonably well with the value predicted from Wranglen's equation. The measured value was approximately 350 $\mu amps/cm^2$. The predicted value calculated from Wranglen's equation is 468 $\mu amps/cm^2$. At the higher velocities, the limiting diffusion current was not obvious. The Wranglen equation predicts I should increase with $V^{.6}$ so that at 9 m/s, a limiting diffusion current of 600 $\mu amps/cm^2$ would be expected.

It is believed that limiting oxygen diffusion currents at the higher velocities are being masked by another reduction reaction. In turbulent flow at 6 m/s, considerable polarization (~.7 volt) was necessary to show a mass transfer limited region on the curve. At 9 m/s, it is reasonable to expect that mass transfer limited behavior would only be obvious at higher values

of overpotential. However, at these higher values of overpotential, another reduction reaction becomes thermodynamically possible and is apparently significant, namely:

$$H_2O + 1e \rightarrow OH^- + 1/2\ H_2$$

In seawater, the redox potential of this reaction is ≈-.715 volt (vs. SCE). Thus, it is hypothesized that the reaction involving the reduction of water is more significant than the reduction of oxygen at higher potentials in high velocity seawater under turbulent flow. The onset of this reaction also prevents experimental verification of the Wranglen expression in high velocity, turbulent flow.

CONCLUSIONS

1. Over the higher velocity regime and flow conditions characteristic of this study (9 to 30 m/s), the increase in corrosion rate with velocity appears to be proportional to velocity raised to the 3.6 power. The increase in corrosion rate with velocity is much larger than would be predicted for a reaction rate controlled by mass transfer of a reacting species through a boundary layer in the fluid. Thus, other factors (e.g. stability of the oxide film) appear to have a larger influence on the corrosion rate at high seawater velocities.

2. The hydrated oxide films that normally form on aluminum alloys in seawater become increasingly unstable with increasing velocity.

3. Under parallel flow conditions like those simulated in this study, corrosion of aluminum alloys changes from a marcopitting mode to a micropitting mode with increasing velocity.

4. Under flow conditions like those obtained in this study, the corrosion potential of the 5456 will exhibit a shift in the active direction with increasing velocity; the corrosion potential of the 1100 alloy will remain fairly constant with increasing velocity.

5. At high seawater velocities, the corrosion rate of aluminum alloys predicted from polarization resistance measurements will be significantly lower than the actual corrosion rate as determined by weight loss measurements.

6. Under flow conditions like those obtained in this study, cathodic protection cannot be employed to retard velocity-induced corrosion of aluminum alloys.

7. Aluminum alloys are susceptible to accelerated corrosion as the result of cathodic polarization over the entire velocity range examined in this study.

8. The predominant reduction reaction associated with corrosion of aluminum alloys at higher seawater velocities is probably $H_2O + 1e \rightarrow OH^- + 1/2\ H_2$ rather than $1/2\ O_2 + H_2O + 2e \rightarrow 2(OH)^-$.

ACKNOWLEDGEMENT

The author gratefully acknowledges the financial support of the Office of Naval Research under the project supervision of Dr. P. A. Clarkin.

REFERENCES

1. G. A. Gehring, Jr. & M. H. Peterson, "Corrosion of 5456-H117 Aluminum In High Velocity Seawater", paper #266 presented at the NACE Conference, Atlanta, Georgia, (1979).

2. R. D. Efird, Corrosion, Vol. 33, No. 1 January, (1977).

3. I. Cornet & V. Kaloo, "Temperature and Velocity Effects on the Cathodic Protection of a Steel Disc Rotating in Salt Water", Proc. Third International Congress On Metallic Corrosion, Moscow, III, 83, (1969).

4. B. K. Mahato, S. K. Voora, & L. W. Shemilt, Corrosion Science, 8, 173, (1968).

5. B. C. Syrett, Corrosion, Vol. 32, No. 6, June, (1976).

6. A. C. Makrides, Corrosion, Vol. 18, September, (1962).

7. F. Mansfeld & J. V. Kenkel, Corrosion, Vol. 35, No. 1, January, (1979).

8. V. G. Levich, Physicochemical Hydrodynamics, Prentice-Hall, Englewood Cliffs, (1962).

9. A. Becerra & R. Darby, Corrosion, Vol. 30, No. 5, May, (1974).

10. J. E. Draley & W. E. Ruther, Corrosion, Vol. 12, (1956).

11. Metals Handbook, Vol. 1, American Society of Metals, Metals Park, Ohio, 8th Edition, p. 916.

12. M. Stern & A. L. Geary, Jnl. Elec. Chem. Soc., Vol. 104, No. 56, (1957).

13. F. Mansfeld, Corrosion, Vol. 29, No. 10, October, (1973).

14. F. Mansfeld & K. B. Oldham, Corrosion Science, Vol. 11, (1971).

15. G. A. Gehring, Jr., "Performance of Selected Marine Coatings Exposed to High Velocity Seawater", a paper to be published in the Journal of Coatings Technology, February (1980).

16. J. Perkins, W. H. Luebke, K. J. Graham, & J. M. Todd, Jnl. Elec. Chem. Soc., Vol. 124, No. 6, (1977).

17. J. A. Davis & G. A. Gehring, "Pitting Behavior of Aluminum Alloys in High Velocity Seawater", a paper presented at the Annual Conference of the Electrochemical Society, October, (1976).

18. G. Leumer, R. P. Schack, K. J. Graham, and J. Perkins, "The Effect of Flow Structure on Corrosion", Naval Postgraduate School Report No. NPS-69PS-78-004, May, (1978).

19. G. Wranglen & O. Nilson, Electrochem. Acta, 7, (1962).

20. M. G. Fontana & N. D. Greene, Corrsion Engineering, McGraw-Hill, New York, (1967), p. 335.

TABLE I - TYPICAL COMPOSITION OF 5456-H117 ALUMINUM

wt,%

Al	Mg	Mn	Cr	Cu	Zn	Ti	Si+Fe	Other
Bal	4.7-5.5	.50-1.0	.05-.20	.10 max.	.25 max.	.20 max	.40 max.	.15 max.

TABLE II - SUMMARY OF TEST CONDITIONS FOR EACH TEST RUN

Test Run #1

Velocity - 30 m/s
Materials - Three (3) panels 1100 Al; one (1) panel 5456 Al cathodically polarized @ - 1.00 volt vs. SCE
Time of Exposure - 795 hours continuous
Average Seawater Temperature - 19.4°C
Average Seawater Salinity - 30,005 ppm
Average Seawater Dissolved O_2 - 7.34 ppm
Average Seawater pH - 8.1
Average Seawater Turbidity - 14.2 JTU

Test Run #2

Velocity - 30 m/s
Materials - One (1) 5456 Al panel freely corroding;- One (1) 5456 Al panel coupled to a zinc anode; one (1) 5456 Al panel cathodically polarized to -1.40 volts vs SCE; and one (1) 5456 Al panel cathodically polarized to -1.80 volts vs SCE. Current to each panel was applied from zinc anodes mounted directly across from the test panels in the opposite wall of the channel. The two higher cathodic potentials were achieved using an auxiliary DC power supply.
Time of Exposure - 721 hours continuous
Average Seawater Temperature - 14.1°C
Average Seawater Salinity - 32,400 ppm
Average Seawater Dissolved O_2 - 8.2 ppm
Average Seawater pH - 8.0
Average Seawater Turbidity - 17.8 JTU

Test Run #3

Velocity - 18, 15, 12, 9, 6, & 3 m/s
Materials - At each velocity, four (4) 1100 Al panels and one (1) 5456 Al panel
Time of Exposure - 779 hours continuous
Average Seawater Temperature - 9.6°C
Average Seawater Salinity - 33,190 ppm
Average Seawater Dissolved O_2 - 10.3 ppm
Average Seawater pH - 7.9
Average Seawater Turbidity - 24.1 JTU

TABLE II CONT'D

Test Run #4

Velocity - 18, 15, 12, 9, 6 & 3 m/s
Materials - At each velocity, three (3) 5456 Al panels - one coupled to a zinc anode and the other two cathodically polarized at different levels of applied current.
Time of Exposure - 859 hours continuous
Average Seawater Temperature - 17.5°C
Average Seawater Salinity - 32,950 ppm
Average Seawater Dissolved O_2 7.94 ppm
Average Seawater pH - 7.9
Average Seawater Turbidity - 15 JTU

TABLE III - COMPARISON OF CORROSION RATES FOR 5456 ALLOY
(WEIGHT LOSS VERSUS POLARIZATION RESISTANCE)

Velocity	Corrosion Rate (Weight Loss)	Corrosion Rate (Polarization Resistance)*
30 m/s	124 mdd	11.85 mdd
18 m/s	13.5 mdd	1.65 mdd
15 m/s	10.6 mdd	.40 mdd
12 m/s	2.2 mdd	.33 mdd
9 m/s	1.4 mdd	.32 mdd
6 m/s	1.4 mdd	.36 mdd
3 m/s	1.4 mdd	.13 mdd

*Corrosion rates predicted from polarization resistance measurements.

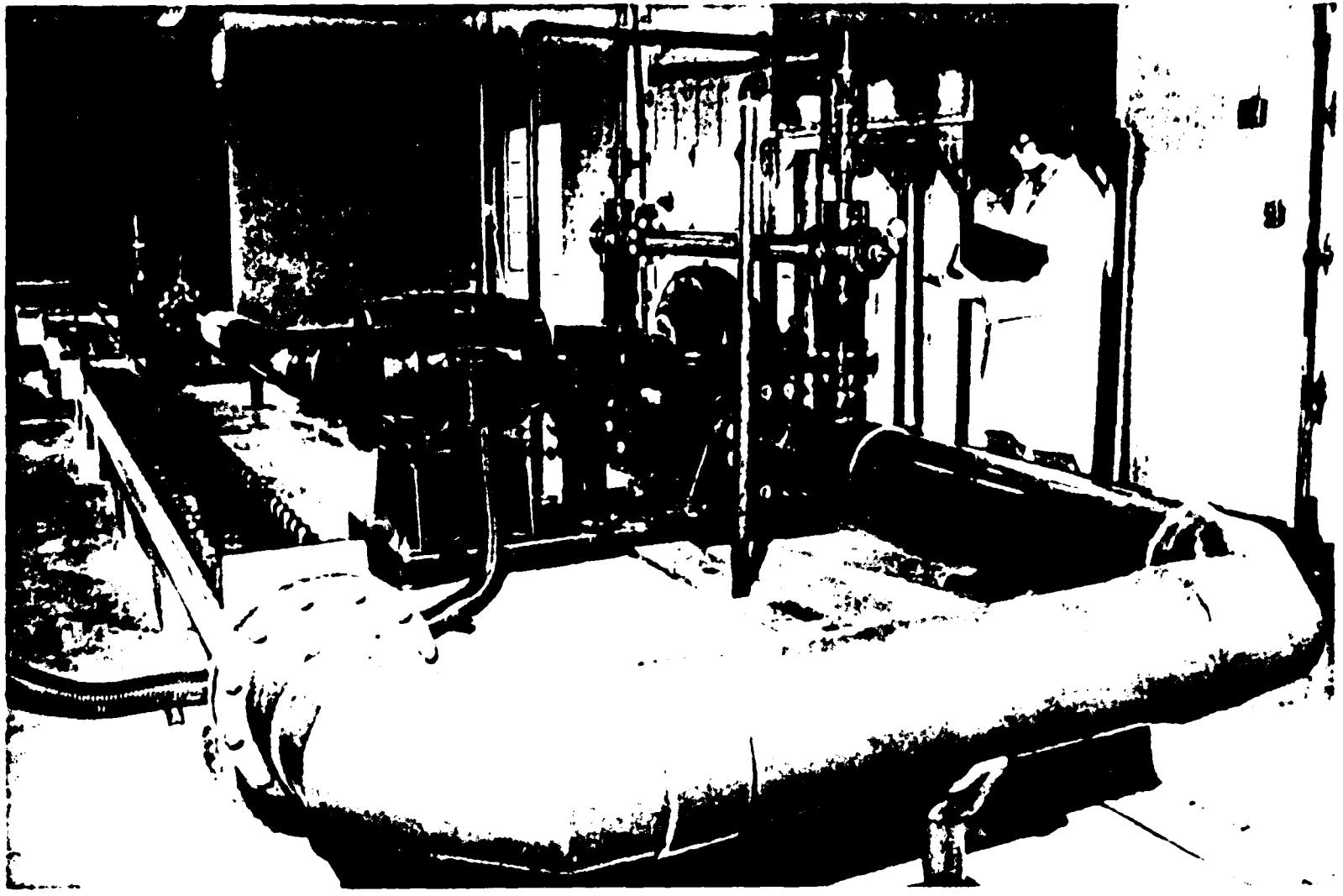

Figure 1 - Flow Channel

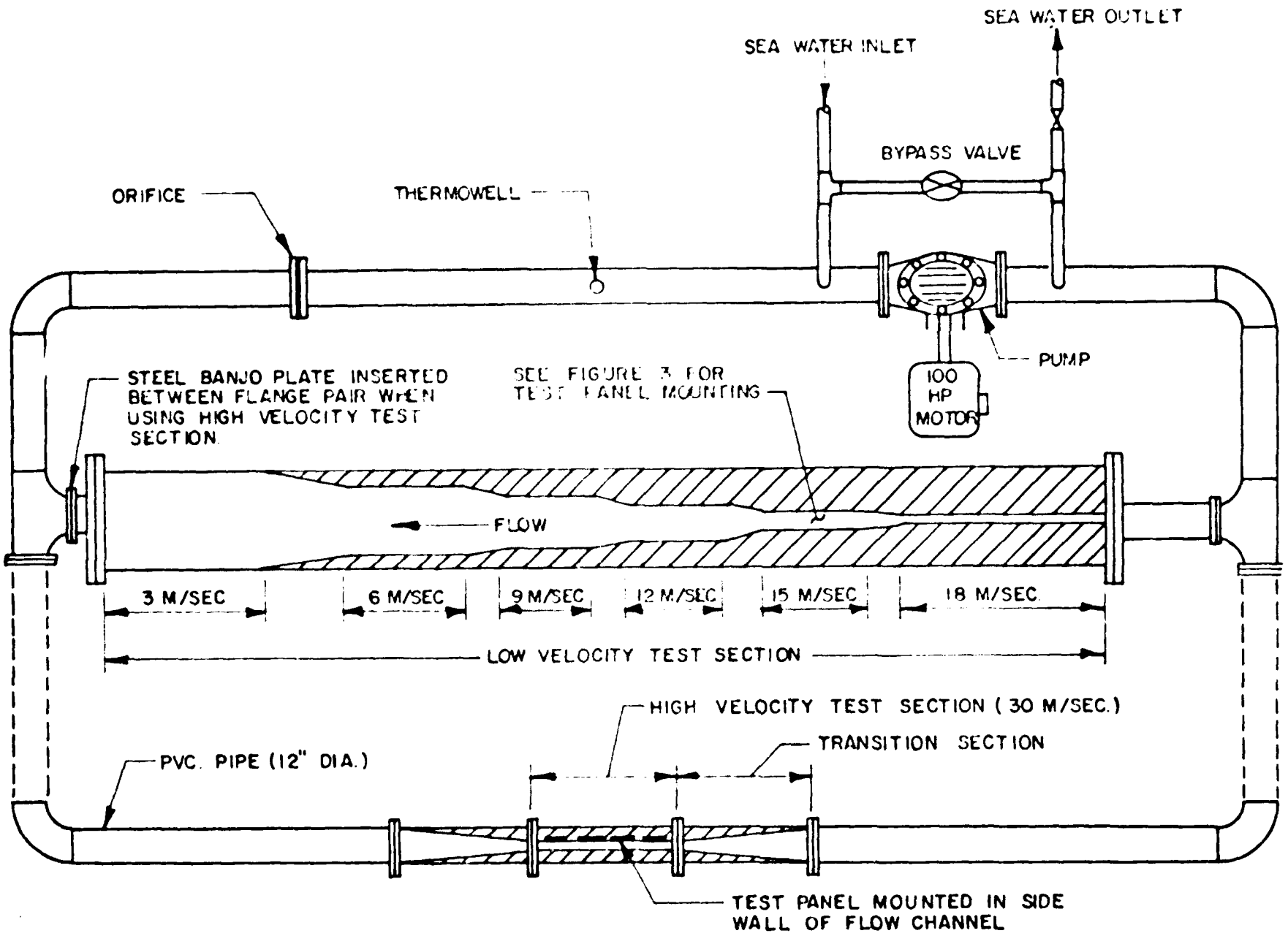

FIGURE 2—SIMPLIFIED SCHEMATIC OF FLOW CHANNEL

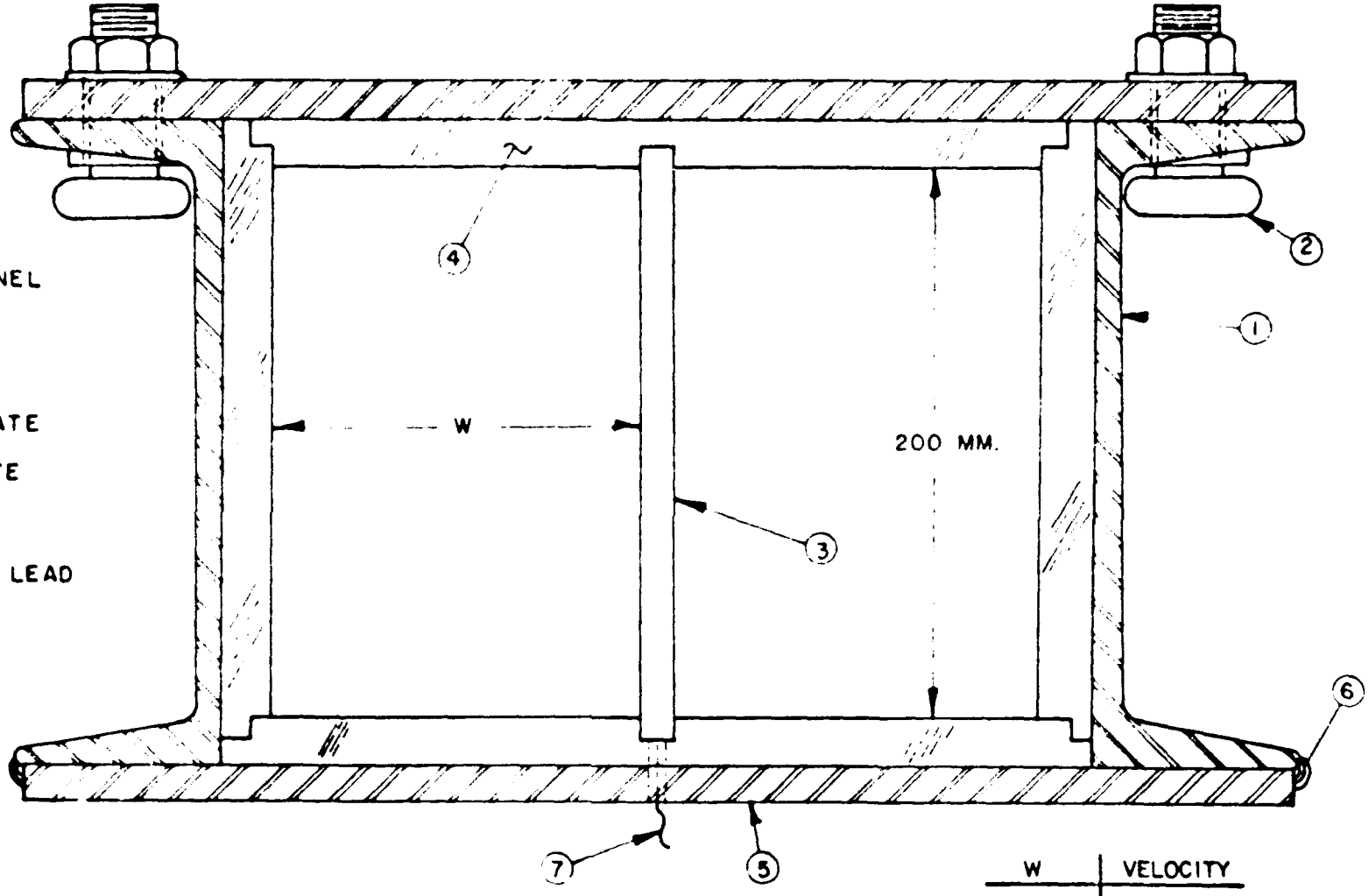

W	VELOCITY
50 MM.	18 M/SEC.
60 MM.	15 M/SEC.
75 MM.	12 M/SEC.
100 MM.	9 M/SEC.
150 MM.	6 M/SEC.
300 MM.	3 M/SEC.

FIGURE 3- CROSS-SECTION VIEW OF TEST PANEL MOUNTED IN FLOW CHANNEL (LOW VELOCITY SECTION)

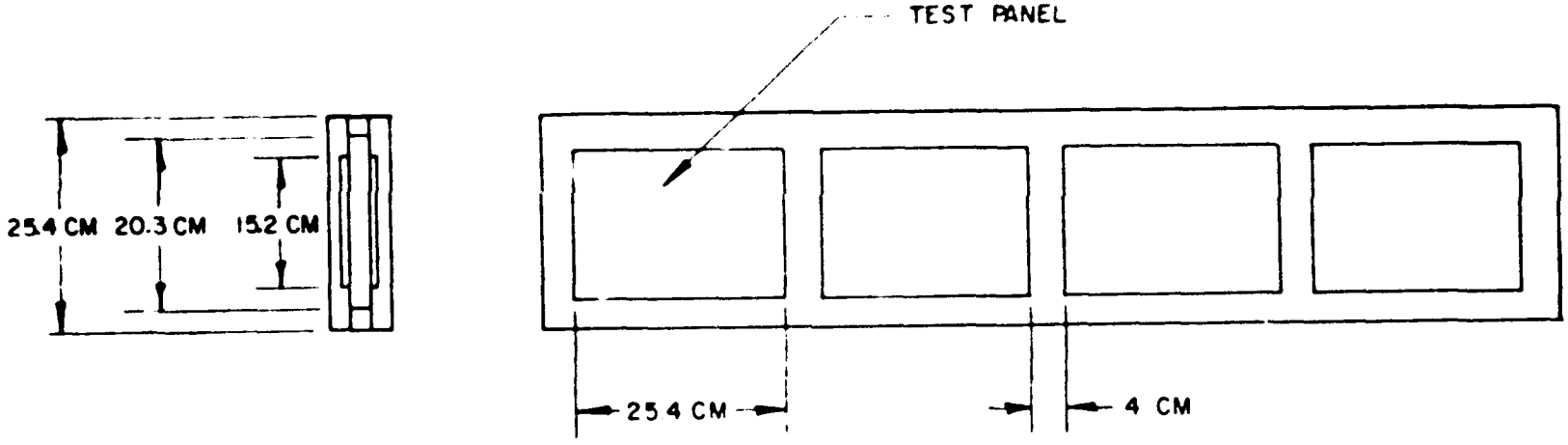

FIGURE 4—ARRANGEMENT OF FLOW CHANNEL AT 30 M/S

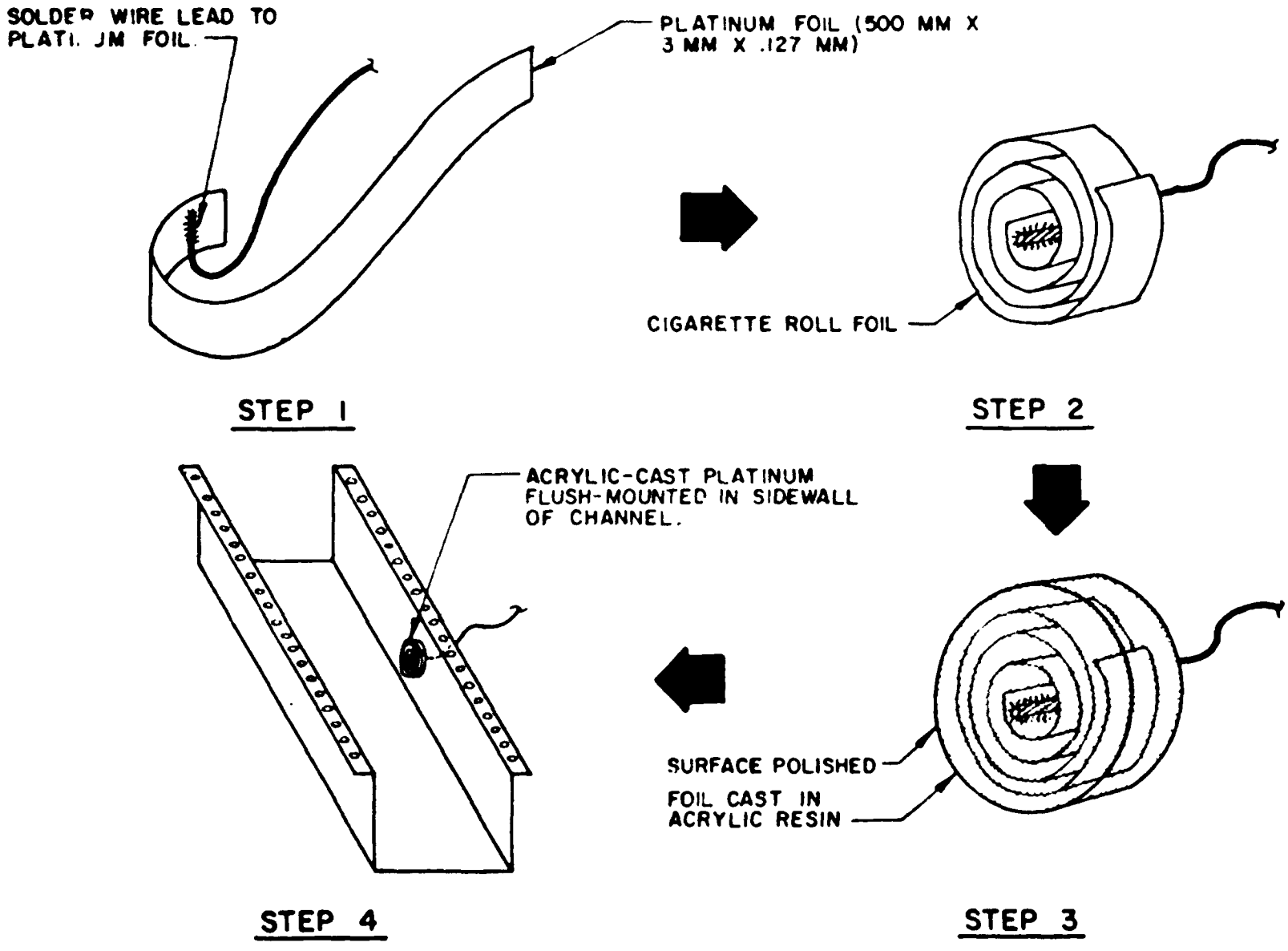

FIGURE 5–PREPARATION AND MOUNTING OF PLATINUM ELECTRODES

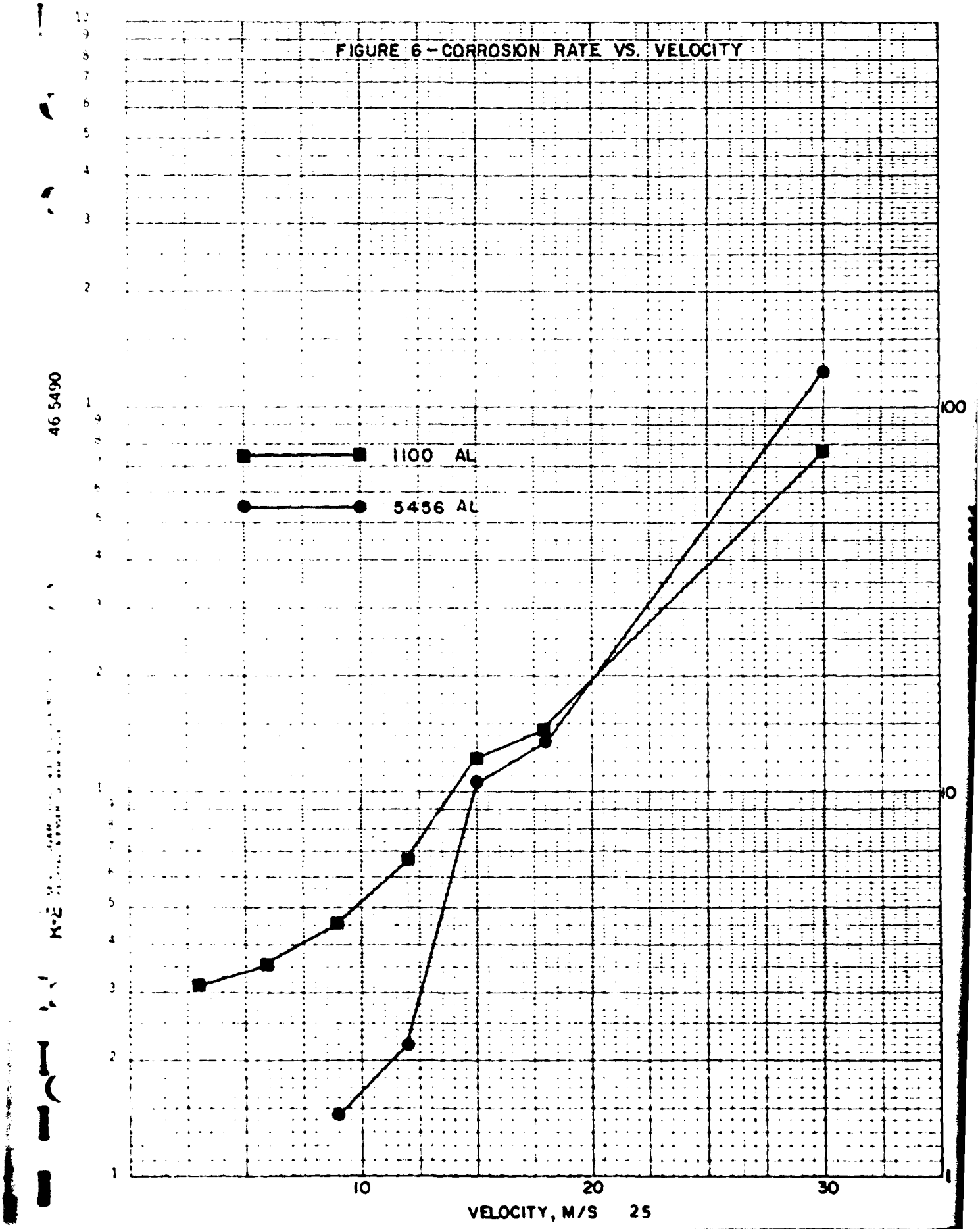
FIGURE 6 – CORROSION RATE VS. VELOCITY
1100 AL
5456 AL
100
10
1
10
20
30
VELOCITY, M/S
25

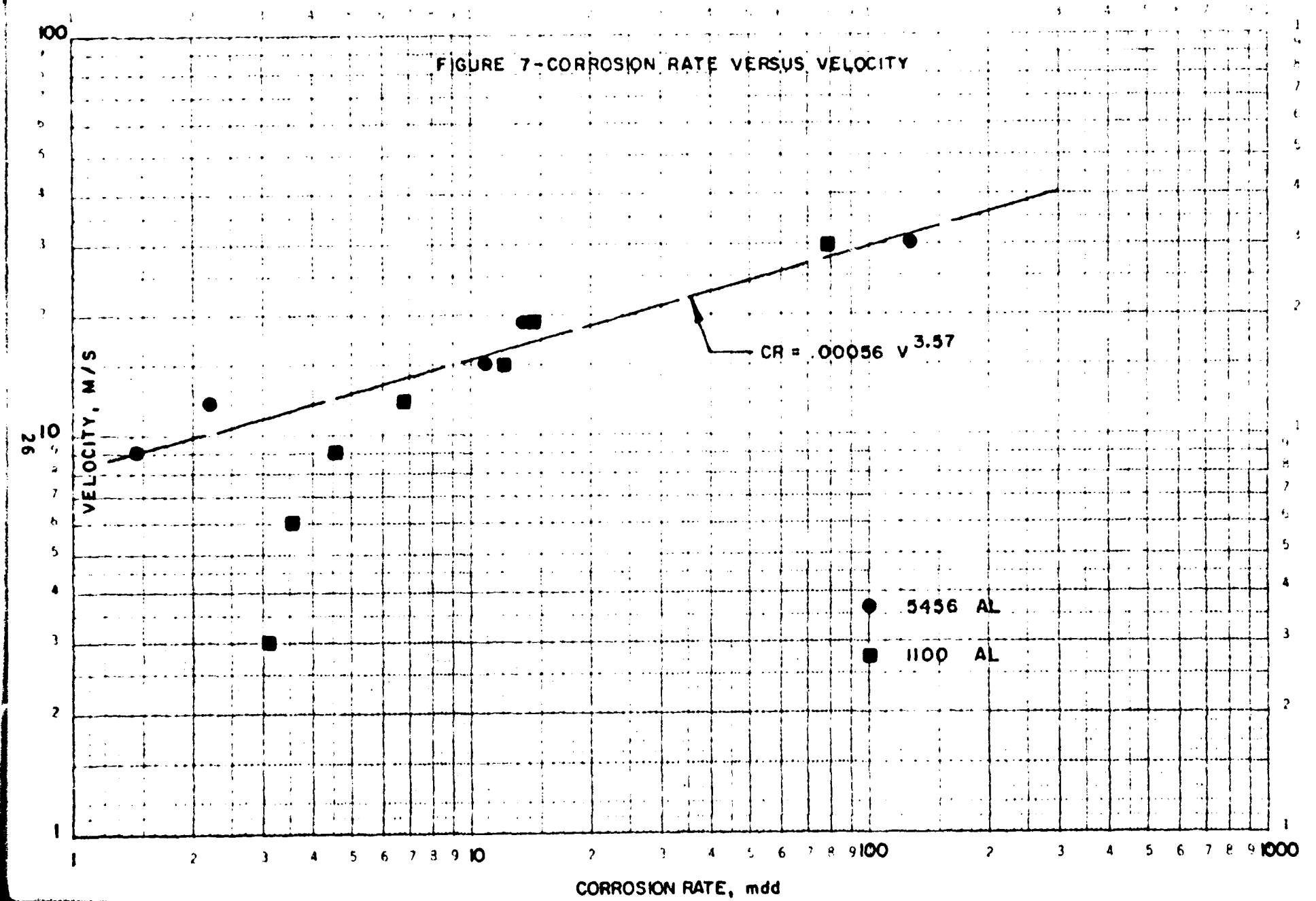
FIGURE 7-CORROSION RATE VERSUS VELOCITY
CR = .00056 V 3.57
5456 AL
1100 AL
VELOCITY, M/S
CORROSION RATE, mdd
100
10
1
1
2
3
4
5
6
7
8
9
10
100
1000

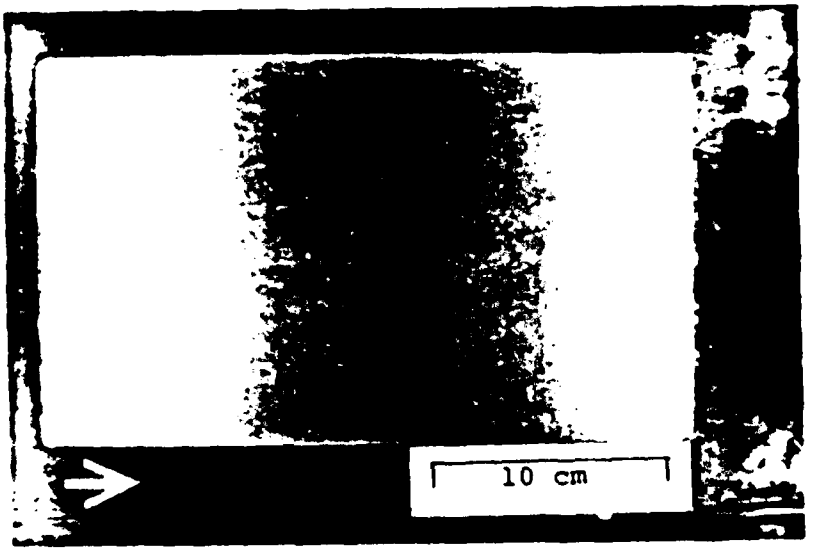

Figure 8 - Macroappearance of 5456 Test Panel After Exposure to Seawater Flowing At 30 m/s For 795 Hours.

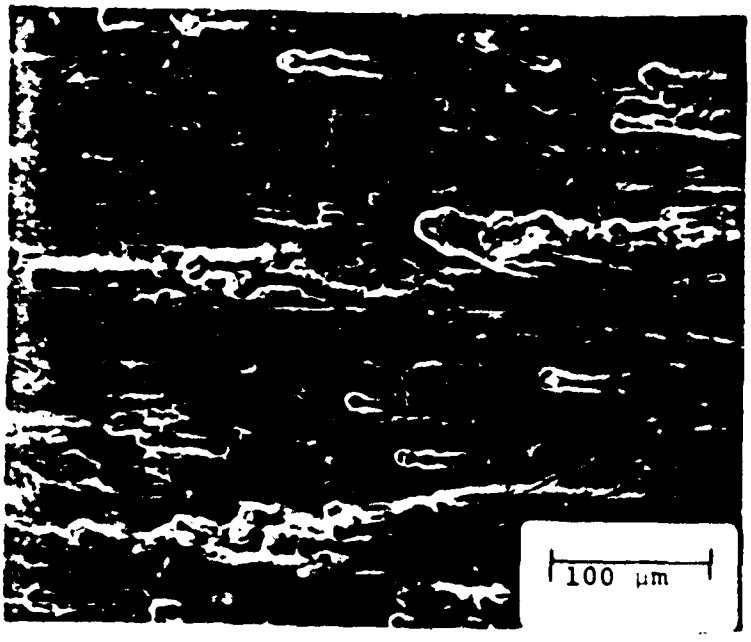

a.

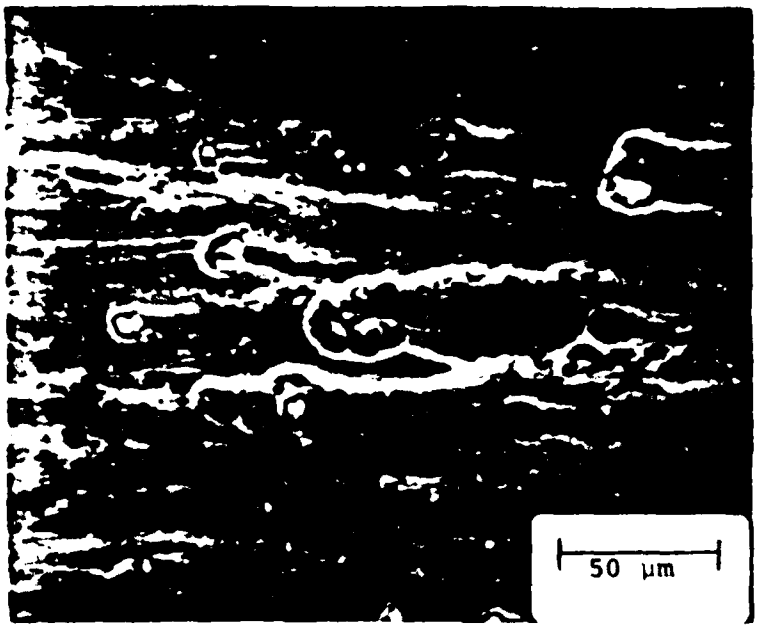

b.

Figure 9 - SEM Micrographs Showing Preferential Pitting At Intermetallic Particles - 5456 AL Exposed For 721 Hours to Flowing Seawater At 30 m/s (Flow was left to right).

Figure 10 - High Velocity Corrosion/Erosion of 5456-H117 Aluminum

Step 1

Pitting initiates in a uniform mode about an intermetallic particle due to galvanic action.

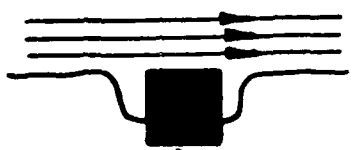

Step 2

As a result of localized pitting combined with general surface attack, the intermetallic particle begins to protrude into the flow stream.

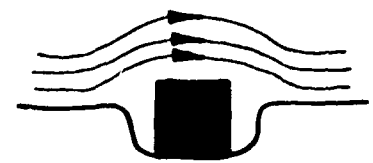

Step 3

This gives rise to greater turbulence immediately downstream of the particle and consequently the pitting rate in this area accelerates.

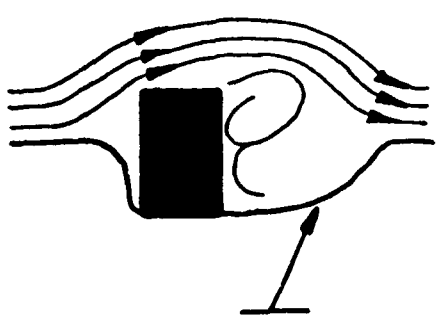

Accelerated pitting downstream of particle.

Step 4

Eventually, the intermetallic particle is sufficiently undermined by corrosion that the hydrodynamic forces are sufficient to "pop" the particles from the matrix. Pitting corrosion in the remaining "hole" then slows down because of the loss of the particle and because of possible flow stagnation in the hole. Gradually, a uniform profile is reestablished. Macroscopically, this accounts for the very uniform loss of metal as corrosion/erosion proceeds.

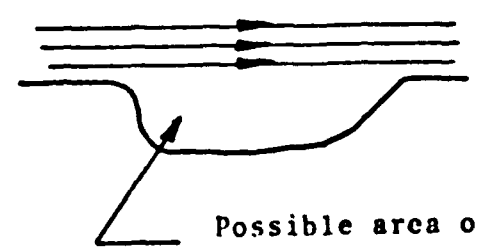

Possible area of stagnant flow.

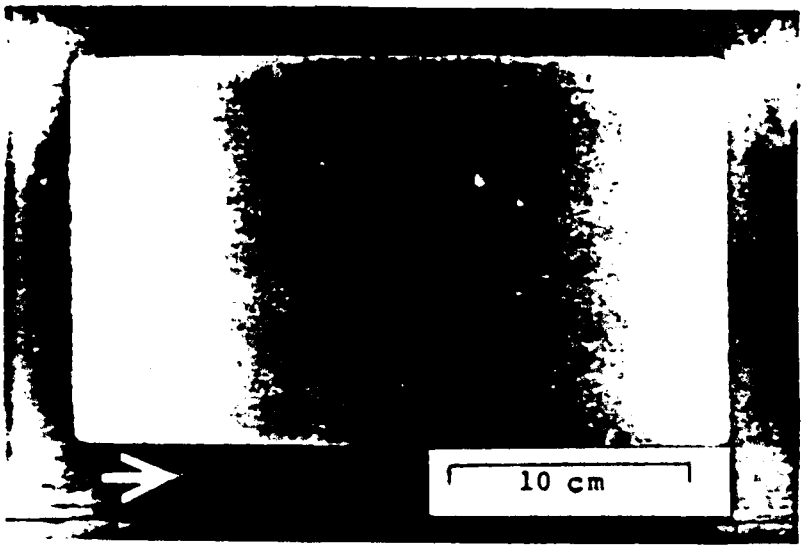

Figure 11 - Macroappearance of 1100 Test Panel After Exposure to Seawater Flowing At 30 m/s For 795 Hours.

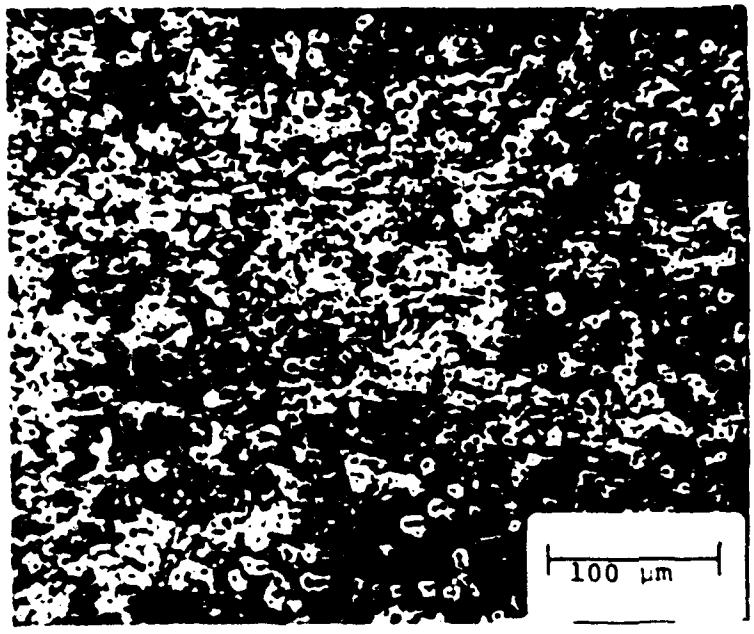

a.

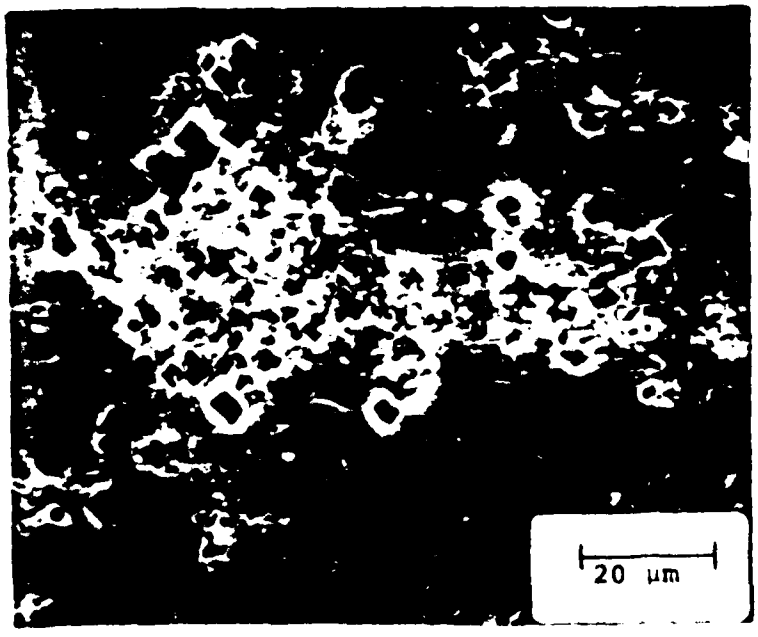

b.

Figure 12 - SEM Micrographs Showing Crystallographic Pits - 1100 Al Exposed For 795 Hours To Flowing Seawater At 30 m/s (Flow was left to right).

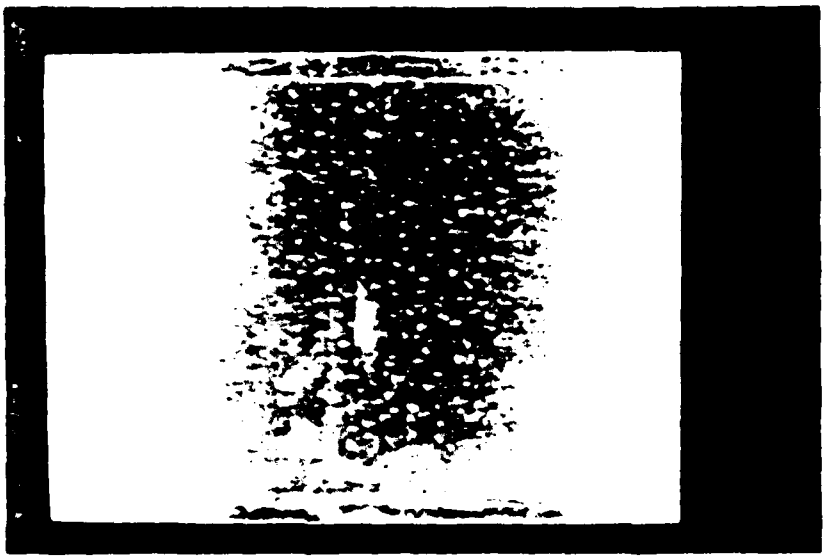

a. 1100 Alloy

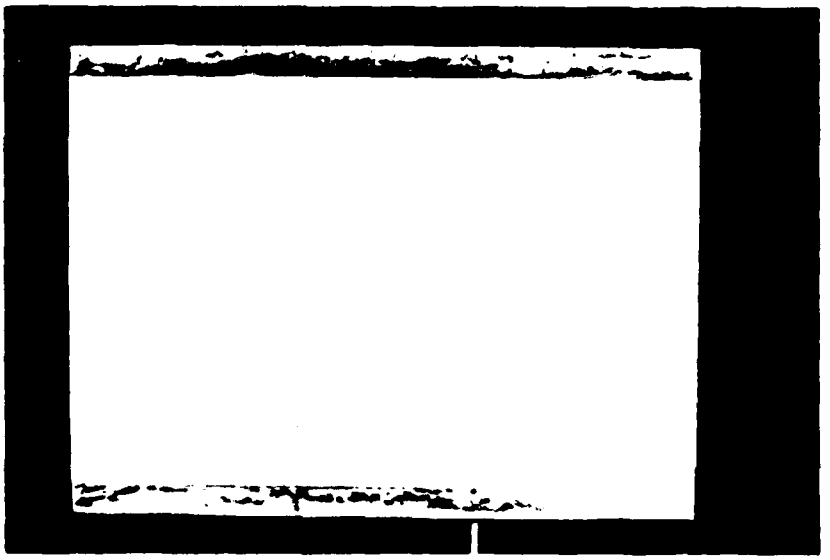

b. 5456 Alloy

Figure 13 - Macroappearance of Aluminum Alloy Test Panels After 779 Hours Exposure To Flowing Seawater At 18 m/s.

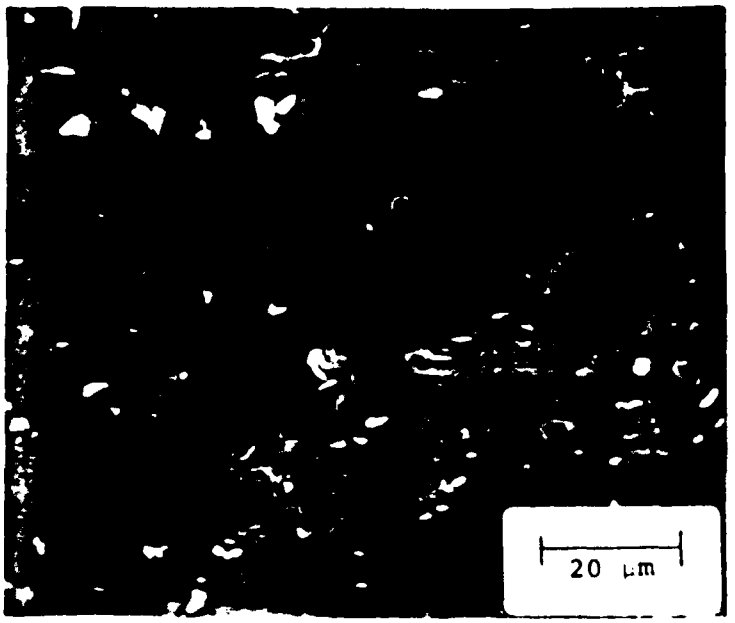

Figure 14 - SEM Micrograph of 1100 Aluminum Alloy Exposed For 779 Hours To Flowing Seawater At 18 m/s (Flow was left to right).

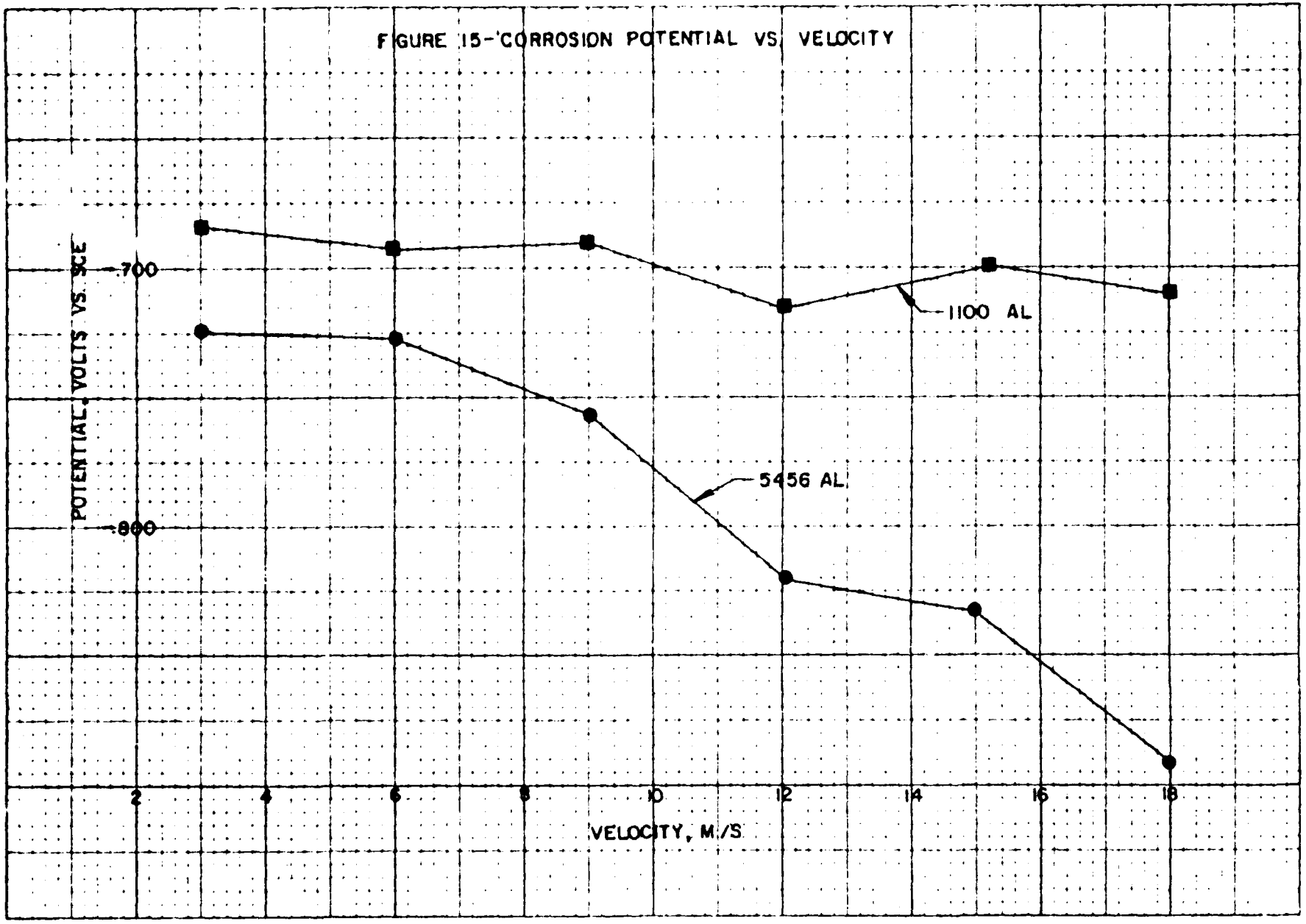
FIGURE 15-'CORROSION POTENTIAL VS. VELOCITY
POTENTIAL, VOLTS VS. SCE
-700
-800
1100 AL
5456 AL
2
4
6
8
10
12
14
16
18
VELOCITY, M/S

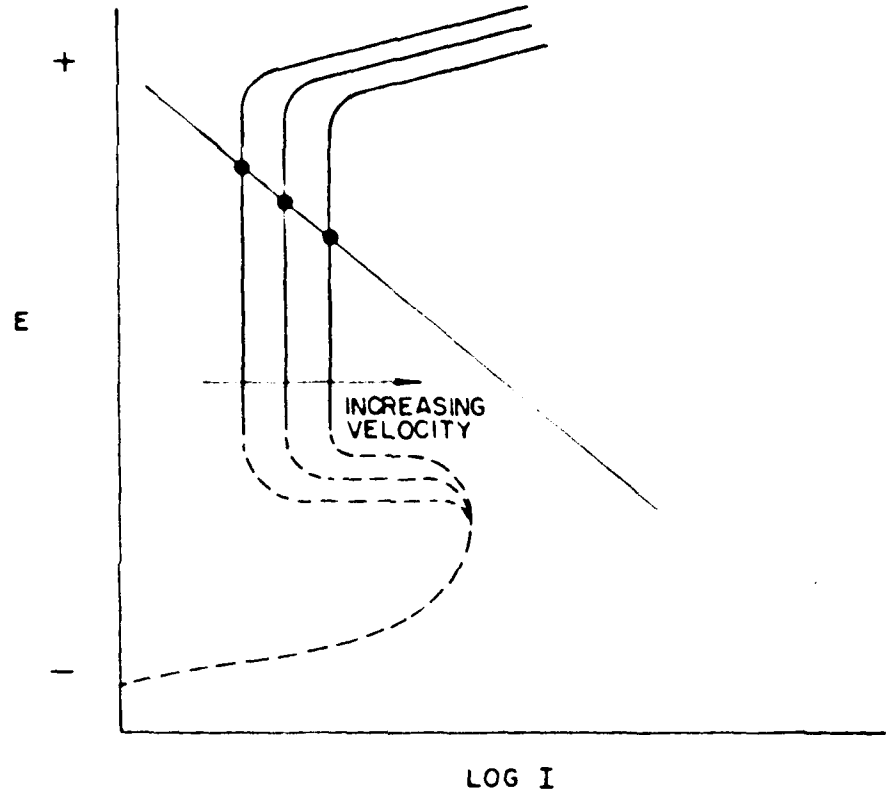

FIGURE 16 – POLARIZATION DIAGRAM SHOWING THE EFFECT OF INCREASING VELOCITY ON THE DIFFUSION-LIMITED ANODIC POLARIZATION CURVE AND THE RESULTING ACTIVE SHIFT IN THE CORROSION POTENTIAL

FIGURE 17-CATHODIC POLARIZATION CURVES FOR 5456 ALLOY

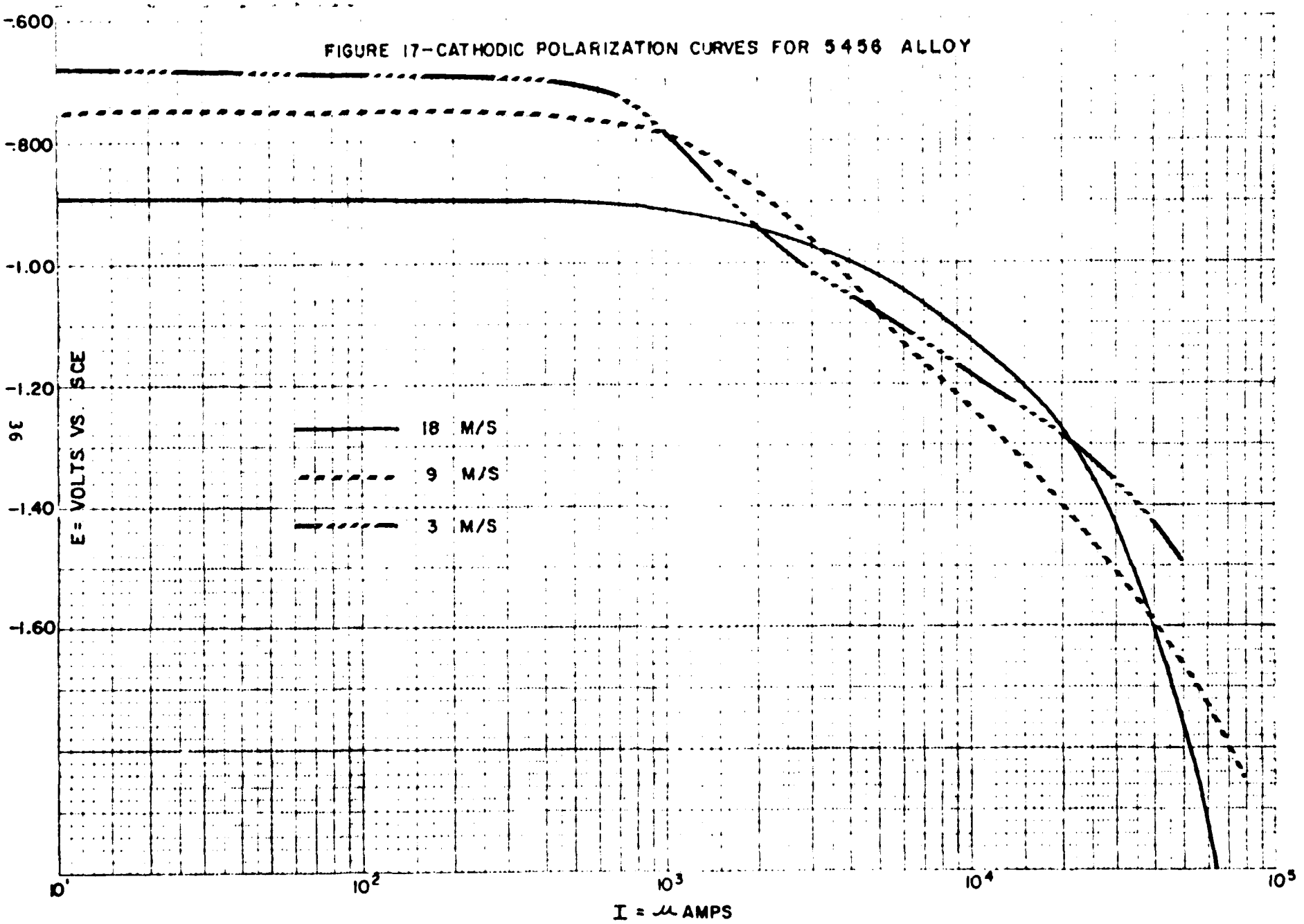

FIGURE 18-CATHODIC POLARIZATION CURVES FOR 1100 ALLOY

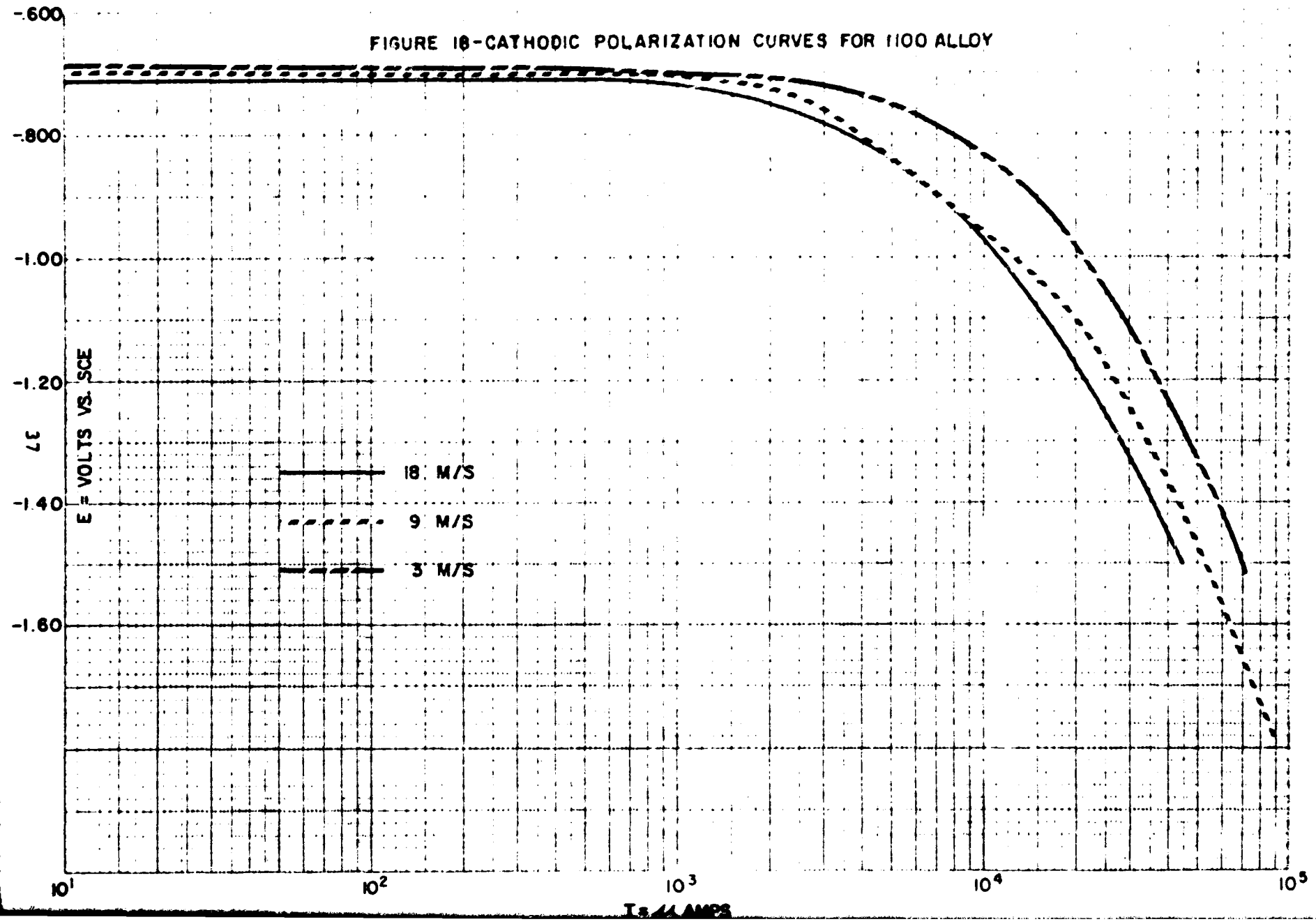

FIGURE 19-CORROSION RATE VS. VELOCITY— ZINC COUPLED 5456 AL & FREELY CORRODING 5456 AL

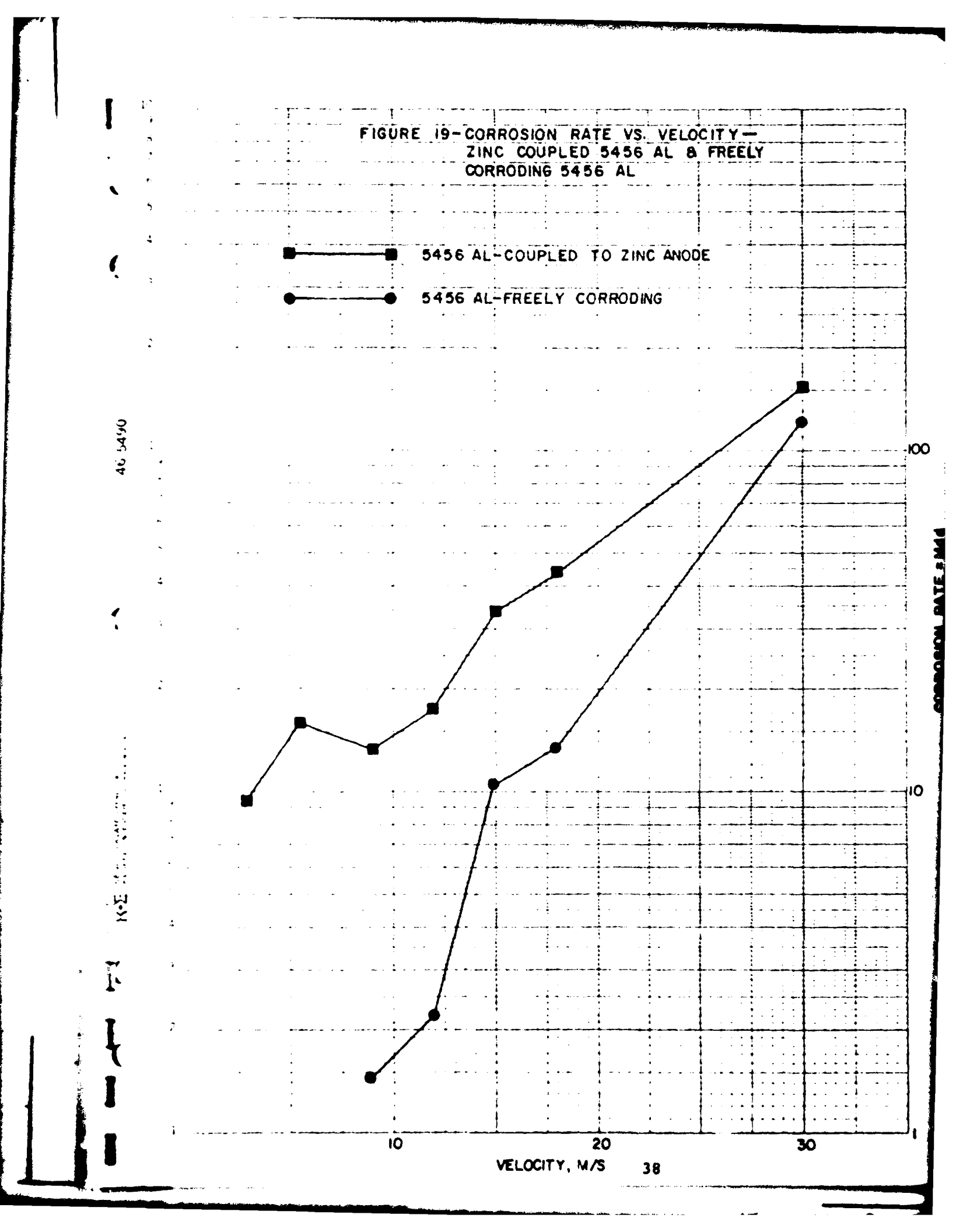

FIGURE 20-5456 AL / ZINC POTENTIALS VS. TIME

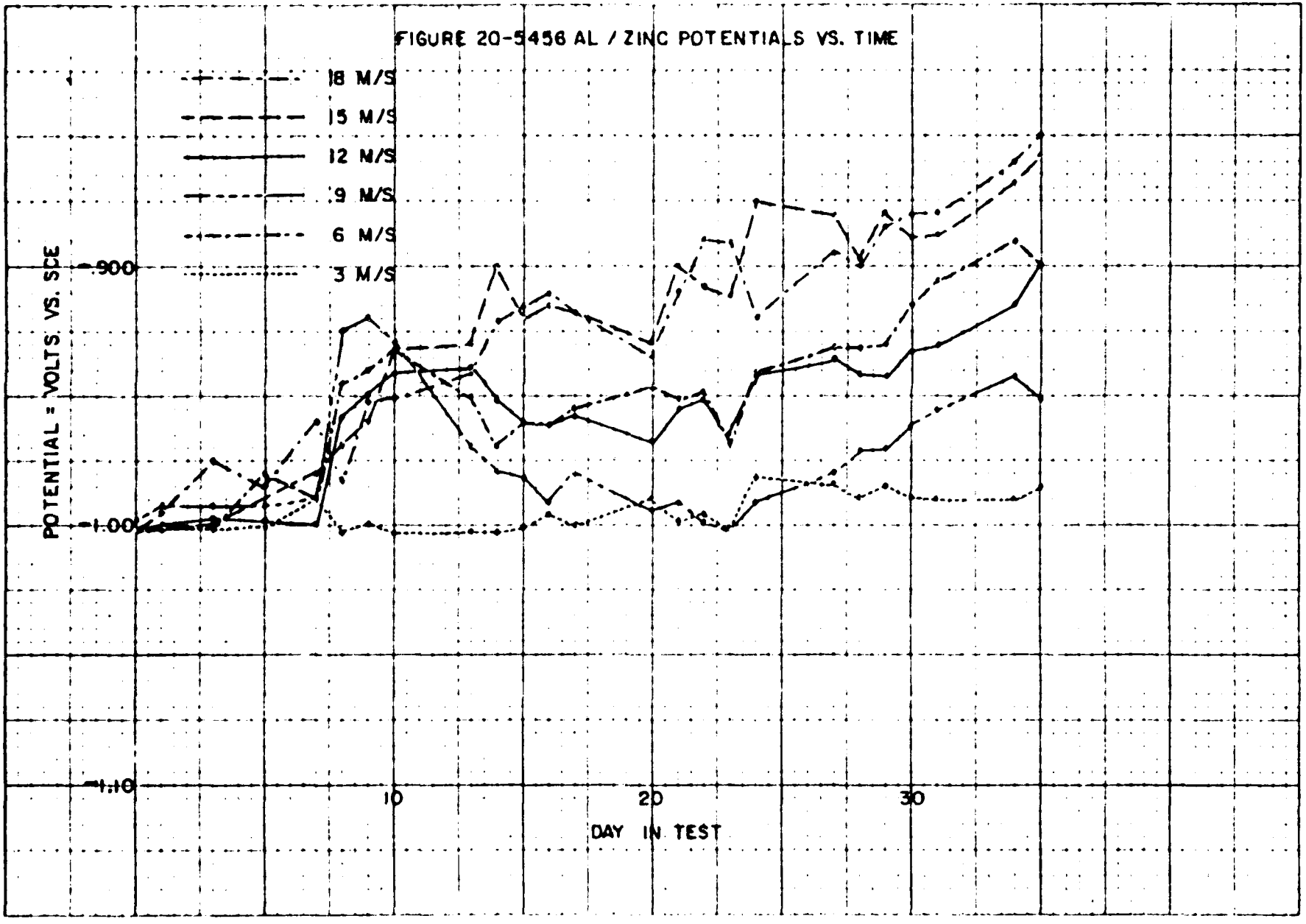

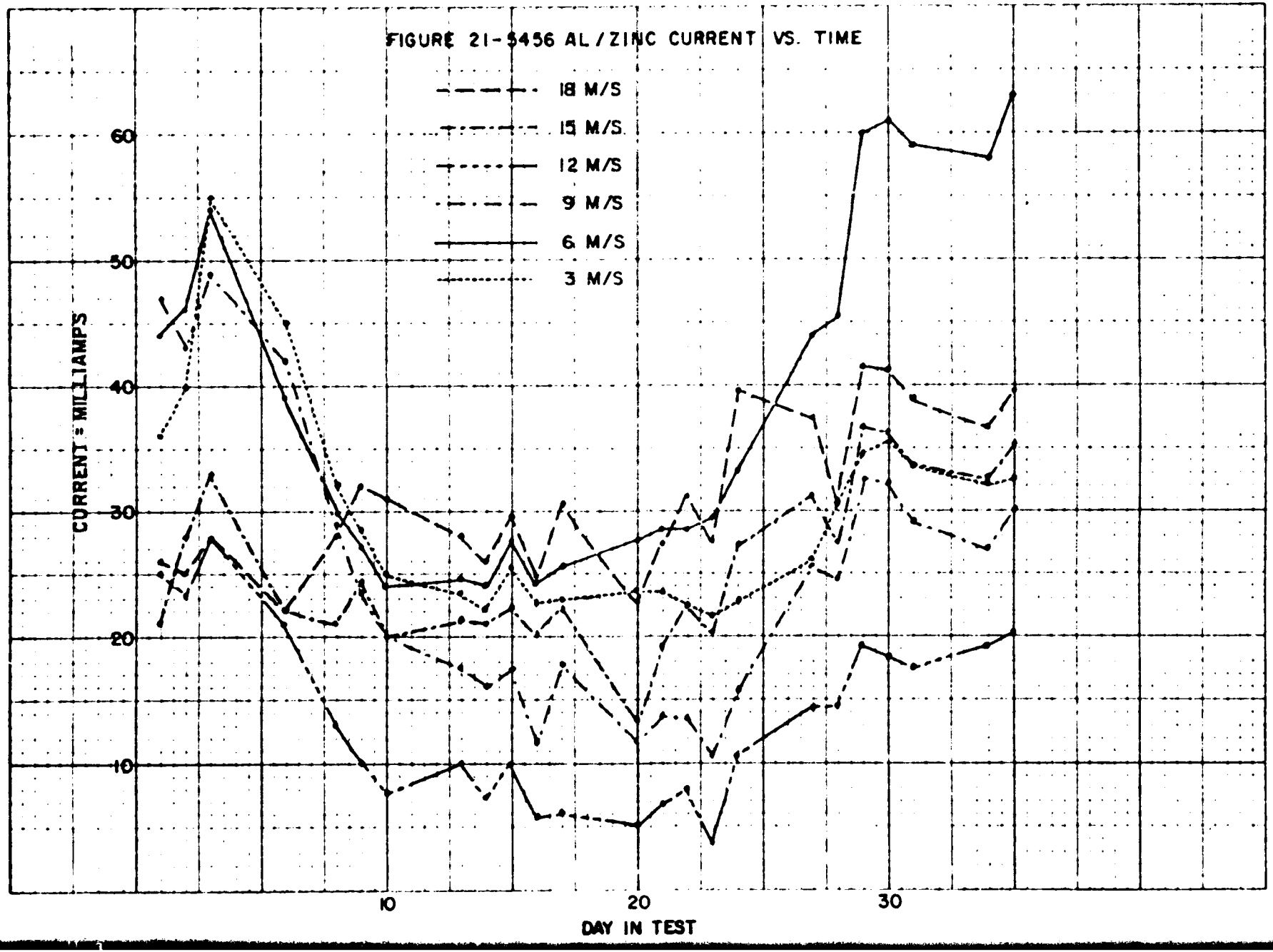

FIGURE 21-5456 AL / ZINC CURRENT VS. TIME

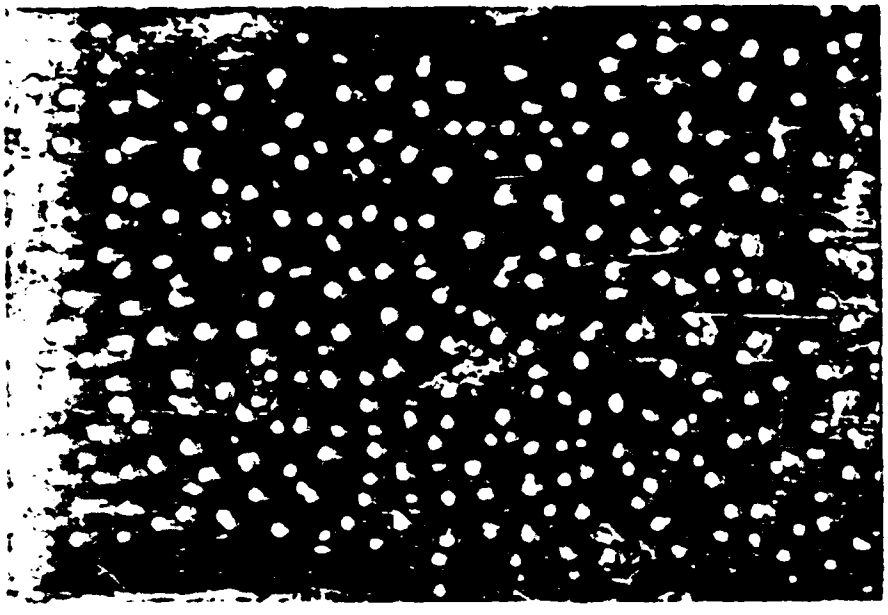

Figure 22 - Macroappearance of Zinc-Coupled Aluminum Test Panel After 859 Hours Exposure To Flowing Seawater At 3 m/s.

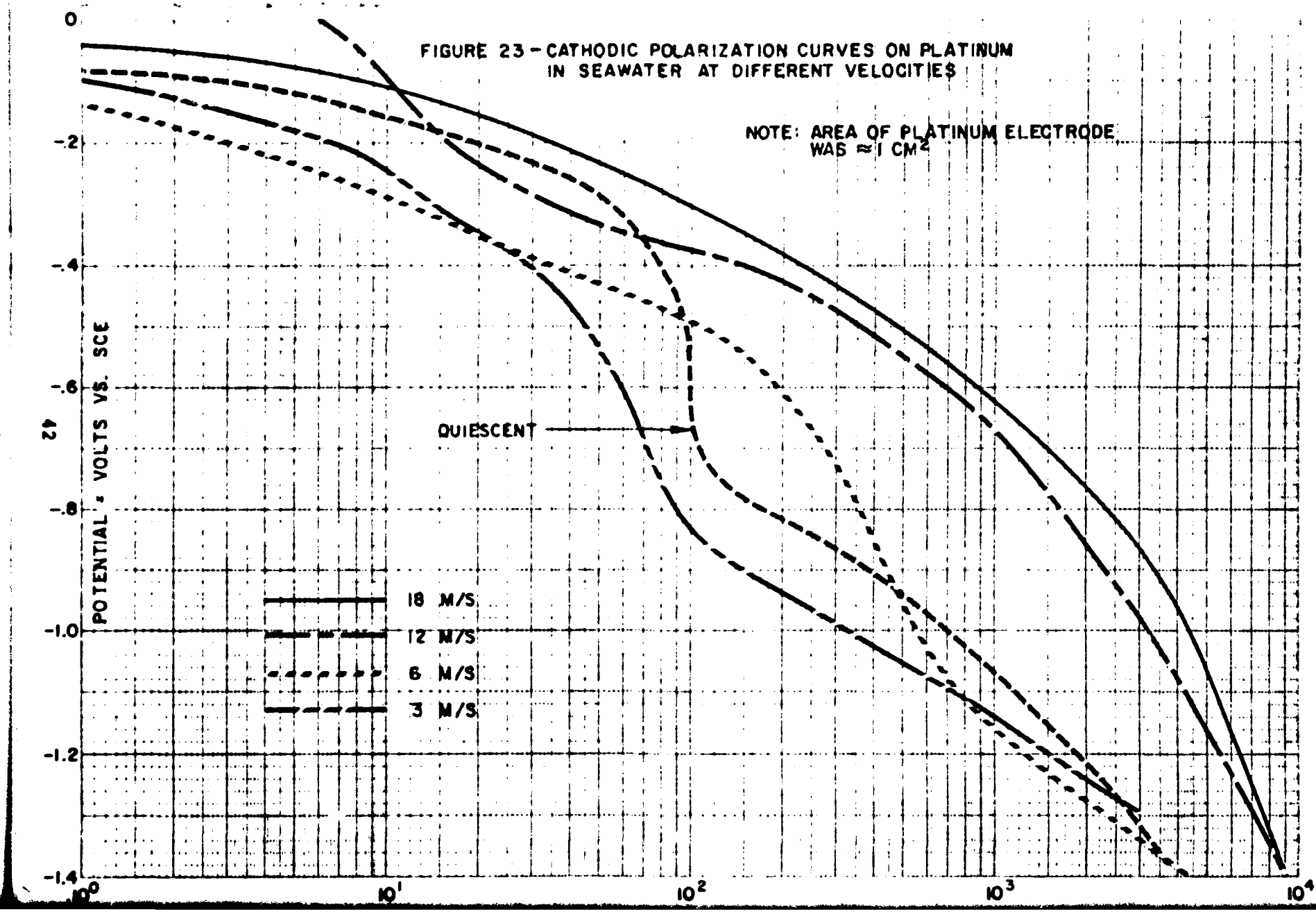
FIGURE 23 - CATHODIC POLARIZATION CURVES ON PLATINUM IN SEAWATER AT DIFFERENT VELOCITIES
NOTE: AREA OF PLATINUM ELECTRODE WAS ≈ 1 CM²
POTENTIAL - VOLTS VS. SCE
0
-.2
-.4
-.6
-.8
-1.0
-1.2
-1.4
QUIESCENT
18 M/S
12 M/S
6 M/S
3 M/S
10⁰
10¹
10²
10³
10⁴